Article

TRANSPARENT PROCESS

THE EMBO JOURNAL

The SAC1 domain in synaptojanin is required for autophagosome maturation at presynaptic terminals

Roeland Vanhauwaert[1,2], Sabine Kuenen[1,2], Roy Masius[3], Adekunle Bademosi[4], Julia Manetsberger[1,2], Nils Schoovaerts[1,2], Laura Bounti[1,2], Serguei Gontcharenko[1,2], Jef Swerts[1,2], Sven Vilain[1,2], Marina Picillo[5], Paolo Barone[5], Shashini T Munshi[6], Femke MS de Vrij[6], Steven A Kushner[6], Natalia V Gounko[1,2,7], Wim Mandemakers[3], Vincenzo Bonifati[3], Frederic A Meunier[4], Sandra-Fausia Soukup[1,2,*] & Patrik Verstreken[1,2,**]

Abstract

Presynaptic terminals are metabolically active and accrue damage through continuous vesicle cycling. How synapses locally regulate protein homeostasis is poorly understood. We show that the presynaptic lipid phosphatase synaptojanin is required for macroautophagy, and this role is inhibited by the Parkinson's disease mutation R258Q. Synaptojanin drives synaptic endocytosis by dephosphorylating PI(4,5)P_2, but this function appears normal in *Synaptojanin^{RQ}* knock-in flies. Instead, R258Q affects the synaptojanin SAC1 domain that dephosphorylates PI(3)P and PI(3,5)P_2, two lipids found in autophagosomal membranes. Using advanced imaging, we show that *Synaptojanin^{RQ}* mutants accumulate the PI(3)P/PI(3,5)P_2-binding protein Atg18a on nascent synaptic autophagosomes, blocking autophagosome maturation at fly synapses and in neurites of human patient induced pluripotent stem cell-derived neurons. Additionally, we observe neurodegeneration, including dopaminergic neuron loss, in *Synaptojanin^{RQ}* flies. Thus, synaptojanin is essential for macroautophagy within presynaptic terminals, coupling protein turnover with synaptic vesicle cycling and linking presynaptic-specific autophagy defects to Parkinson's disease.

Keywords correlative light and electron microscopy; induced pluripotent stem cells; Parkinson's disease; single-molecule tracking; synapse
Subject Categories Autophagy & Cell Death; Neuroscience
DOI 10.15252/embj.201695773 | Received 22 September 2016 | Revised 25 February 2017 | Accepted 1 March 2017 | Published online 22 March 2017
The EMBO Journal (2017) 36: 1392–1411

Introduction

Presynaptic terminals are often distantly located from the neuronal cell body, hampering rapid transport of components between these subcellular compartments (Paus *et al*, 2014). Despite this physical separation, synapses maintain a functional protein pool to support efficient information transfer. They must do so even under conditions of intense synaptic activity that place high metabolic energy demands on this area of the cell. However, the mechanisms that regulate and maintain protein homeostasis at synapses are poorly characterized. Furthermore, impaired synaptic protein homeostasis is implicated in neurodegeneration where combined failure of protein quality control systems and synaptic defects are recurrent themes (Selkoe, 2002; Burke & O'Malley, 2013; Soukup *et al*, 2013).

Parkinson's disease (PD) is a common neurodegenerative condition characterized by the loss of substantia nigra neurons alongside broader pathology in most patients. While ~90% of PD cases are idiopathic, at least 10% have a family history of disease and several causative genes are identified (Thomas & Beal, 2007; Klein & Westenberger, 2012). While these PD genes encode a functionally diverse set of proteins, there is an emerging theme that several act on synaptic vesicle trafficking (Vanhauwaert & Verstreken, 2015; Lepeta *et al*, 2016; Schirinzi *et al*, 2016). However, the nature and degree of synaptic vesicle trafficking impairment that is caused by pathogenic mutations remains unclear.

Synaptojanin 1 (Synj1) is a lipid phosphatase that is essential for synaptic vesicle trafficking (McPherson *et al*, 1996; Cremona *et al*, 1999; Harris *et al*, 2000; Verstreken *et al*, 2003). It is also mutated in several different families with hereditary early-onset PD (Krebs

1 VIB Center for Brain & Disease Research, Leuven, Belgium
2 Department of Human Genetics, Leuven Institute for Neurodegenerative Disease (LIND), KU Leuven, Leuven, Belgium
3 Department of Clinical Genetics, Erasmus MC, Rotterdam, The Netherlands
4 Clem Jones Centre for Ageing Dementia Research, Queensland Brain Institute, The University of Queensland, Brisbane, Qld, Australia
5 Department of Medicine and Surgery, Center for Neurodegenerative Diseases (CEMAND), University of Salerno, Salerno, Italy
6 Department of Psychiatry, Erasmus MC, Rotterdam, The Netherlands
7 Electron Microscopy Platform, VIB Bio-Imaging Core, Leuven, Belgium
*Corresponding author. Tel: +32 1637 7035; E-mail: sandra.soukup@cme.vib-kuleuven.be
**Corresponding author. Tel: +32 1633 0018; E-mail: patrik.verstreken@cme.vib-kuleuven.be

et al, 2013; Quadri *et al*, 2013; Olgiati *et al*, 2014; Kirola *et al*, 2016). Synj1 is evolutionarily well conserved and enriched at synapses (Cremona *et al*, 1999; Harris *et al*, 2000; Verstreken *et al*, 2003; Van Epps *et al*, 2004). The protein has two different lipid phosphatase domains, 5-phosphatase and SAC1, that target different phosphoinositide phosphate (PtdInsP) species. The 5-phosphatase domain specifically hydrolyzes phosphates on the 5′ position of the inositol ring and has a preference for $PI(4,5)P_2$ as a substrate (Whisstock *et al*, 2000; Tsujishita *et al*, 2001). In contrast, the SAC1 domain hydrolyzes PI(3)P, PI(4)P, and $PI(3,5)P_2$ (Guo *et al*, 1999; Zhong *et al*, 2012).

Differently phosphorylated PtdInsP lipids concentrate on different organelles or membrane subdomains. Many proteins recognize particular PtdInsP, and thus are recruited to a specific membrane. This underlies the concept that PtdInsP lipids act as molecular tags that confer membrane identity (Wenk & De Camilli, 2004; Di Paolo & De Camilli, 2006; Ueda, 2014; Lauwers *et al*, 2016; Marat & Haucke, 2016). For example, patches of $PI(4,5)P_2$ at the synaptic membrane bind clathrin adaptors and other endocytic factors to promote synaptic vesicle formation adjacent to active zones. This $PI(4,5)P_2$-dependent binding underlies why Synj1 is essential for synaptic vesicle cycling, whereby the 5-phosphatase domain hydrolysis of $PI(4,5)P_2$ lowers the membrane-binding affinity of endocytic adaptors and uncoats newly formed vesicles (Cremona *et al*, 1999; Gad *et al*, 2000; Verstreken *et al*, 2003). Other PtdInsPs are critical as well, for example, PI(4)P in Golgi membranes and PI(3)P in endosomes recruit specific proteins to the surface of these organelles. In addition, PI(3)P and $PI(3,5)P_2$ are essential during the formation of autophagosomes where they are recognized by proteins like Atg18a/WIPI2 that promote autophagosome biogenesis (Simonsen & Tooze, 2009; Noda *et al*, 2010; Dall'Armi *et al*, 2013; Proikas-Cezanne *et al*, 2015).

The PD-causing mutations (R258Q and the newly identified R459P) reside in the Synj1 SAC1 domain (Krebs *et al*, 2013; Quadri *et al*, 2013; Olgiati *et al*, 2014; Kirola *et al*, 2016). The R258Q mutation blocks the dephosphorylation of PI(3)P and PI(4)P, while leaving 5-phosphatase activity against $PI(4,5)P_2$ unaffected (Krebs *et al*, 2013). This strongly implicates disturbed presynaptic PtdInsP signaling in PD pathogenesis. Although, blocking Synj1 5-phosphatase activity in mouse neurons causes severe endocytic defects during intense stimulation. When SAC1 enzymatic function is inhibited, synaptic vesicle cycling is only mildly affected (during weak stimulation) (Mani *et al*, 2007). This suggests the SAC1 and 5-phosphatase domains have distinct presynaptic functions, but currently little is known about which aspects of presynaptic cell biology are controlled by the Synj1 SAC1 domain.

In this work, we show that the Synj1-SAC1 domain drives autophagosome biogenesis within synapses independent from and in parallel to the well-described importance of Synj in endocytosis. We also provide evidence that in both flies and human neurons differentiated from patient-derived induced pluripotent stem cells (iPSC), the Synj1 SAC1 domain removes the $PI(3)P/PI(3,5)P_2$-binding protein, WIPI2/Atg18a, from immature autophagosomes. This function appears analogous to how hydrolysis of $PI(4,5)P_2$ by Synj1 uncoats endocytic vesicles. Together with our recent finding that another synapse-enriched protein, EndophilinA, is essential for synaptic autophagosome biogenesis (Soukup *et al*, 2016), these data highlight that the presynaptic terminal has unique mechanisms to induce and regulate autophagosome formation. Furthermore, these processes appear tightly connected to PD, potentially explaining the recurrent themes of synaptic dysfunction and protein homeostasis defects found in models of this neurodegenerative disease.

Results

The Parkinson's disease mutation R228Q in the synaptojanin 1 SAC1 domain does not affect synaptic vesicle endocytosis at fly excitatory glutamatergic neurons and photoreceptors

SYNJ1 is evolutionarily conserved from yeast to humans (Fig 1A and B). The human Parkinson's disease-causing R258Q mutation in *SYNJ1* blocks the dephosphorylation of specific phosphoinositides including PI(3)P and to assess the functional consequences of this mutation, we used MiMIC technology and knocked in the R228Q mutation (corresponding to the human R258Q) into the endogenous *Drosophila synj* locus ($synj^{RQ}$) (Appendix Fig S1A) (Venken *et al*, 2011; Vilain *et al*, 2014). This $synj^{RQ}$ knock-in allele expresses Synj at a comparable level to the wild-type *synj* locus, indicating that the mutation does not affect protein stability (Appendix Fig S1B, C, and H). We also developed a second system to study Synj function, where we use the UAS/Gal4 system to transgenically overexpress wild-type or R228Q Synj in neurons of *synj* null mutant flies that otherwise lack Synj expression ($synj^{-/-}$; *nSyb > UAS* $synj^{+}$ or $synj^{RQ}$). We confirm similar expression of these transgenically expressed $Synj^{+}$ and $Synj^{RQ}$ proteins [~1.2-fold over the levels produced from the endogenous *synj* locus (Appendix Fig S1D, E, and I)]. We compared the subcellular localization of endogenous Synj against that produced from the R228Q knock-in locus, or transgenically expressed wild-type $Synj^{+}$ and $Synj^{RQ}$ proteins. We find that all concentrate in the presynaptic terminals of the larval neuromuscular junction (NMJ) (Appendix Fig S1F–G″ and J–M″), indicating the mutant protein localizes correctly and similar to the presynaptic protein EndoA (Verstreken *et al*, 2002).

Synj null mutant animals are not viable (Fig 1C), and deletion of *synj* specifically in the eye severely affects the efficiency of synaptic transmission between eye photoreceptors and the brain detected by electroretinogram (ERG) recordings (Fig 1D, arrowheads). As expected, these *Synj* null phenotypes are rescued by neuronal transgenic expression (*nSyb-Gal4*) of wild-type $Synj^{+}$. Surprisingly, however, transgenic expression of the $Synj^{RQ}$ mutant is as effective as the wild-type protein (Fig 1C and D). Since even a partially active mutant might result in rescue of the phenotype when overexpressed, we confirmed that $synj^{RQ}$ knock-in flies are viable and that they too display normal ERGs (Fig 1D). Hence, it appears that the $Synj^{RQ}$ mutant protein retains core Synj activities that are essential for viability and synaptic communication in the eye.

Synj is best defined as the protein that uncoats newly endocytosed synaptic vesicles (Cremona *et al*, 1999; Harris *et al*, 2000; Verstreken *et al*, 2003). To directly examine whether R228Q affects this endocytic function, we performed FM 1-43 fluorescent dye labeling at the excitatory glutamatergic *Drosophila* NMJ. FM 1-43 binds membranes and is incorporated into and labels newly formed synaptic vesicles, thereby labeling synaptic boutons proportional to the amount of vesicle recycling and thus synaptic endocytosis (Ramaswami *et al*, 1994). As previously described, *synj*

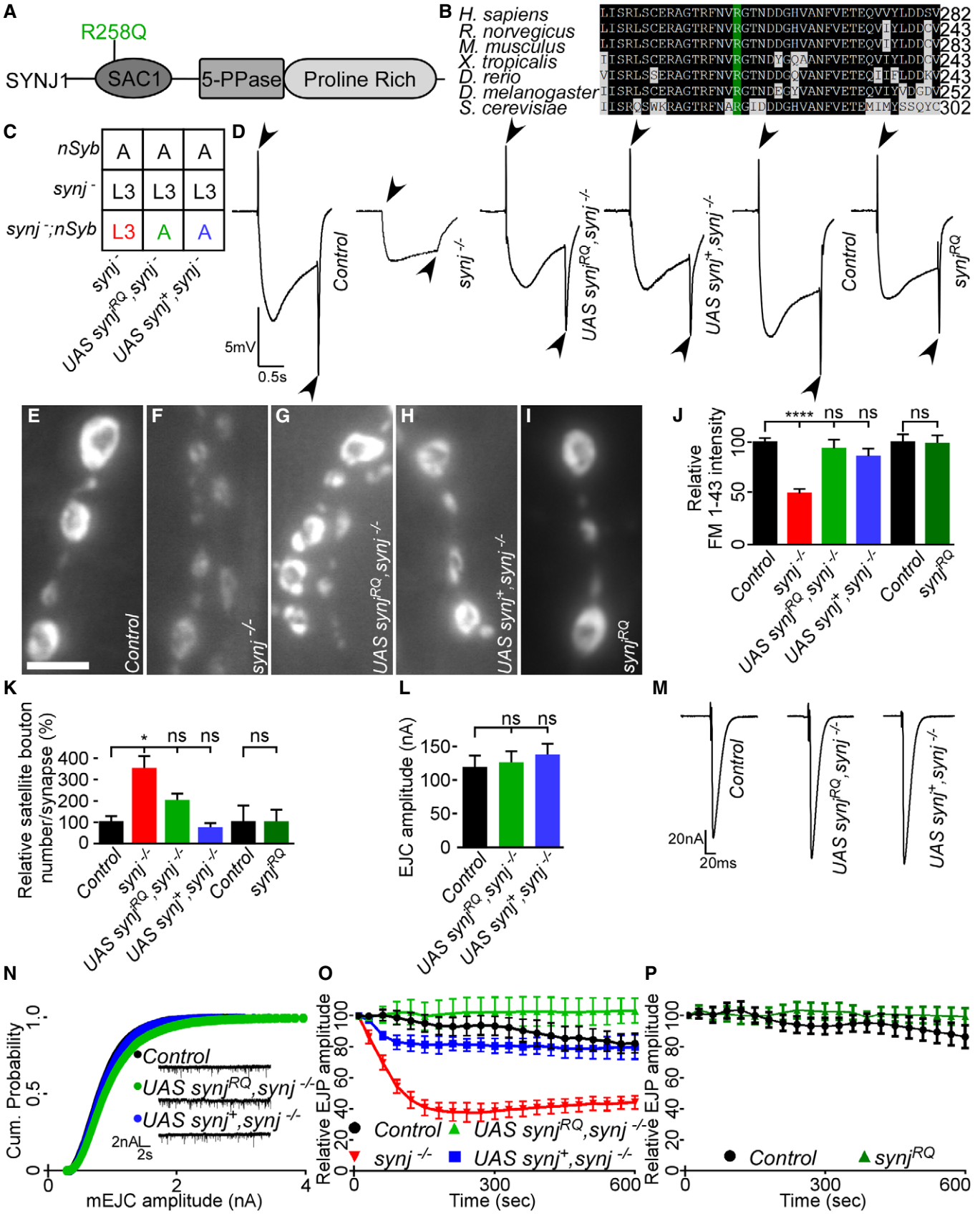

Figure 1.

Figure 1. The Parkinson's disease mutation R228Q in the Synj SAC1 domain does not affect synaptic vesicle cycling.

A Diagram of human Synj1 indicating the two polyphosphoinositide domains (SAC1 and 5-PPase) and the proline-rich domain. The SAC1 domain bears at position 258 an arginine to glutamine amino acid change causative for PD.

B Arginine at position 258 (green) in Synj1 SAC1 domain and the surrounding region are highly conserved from yeast to human (R258 corresponds to R228 in *Drosophila*).

C Table indicating neuronal expression (*nSyb-Gal4*) of Synj^{RQ} and Synj^{+} rescues the lethality of *synj* null mutants (*synj*$^{1/2}$ indicated as *synj*$^{-/-}$), "A" and "L3" indicate lethality at the "adult stage" and at the "third-instar larval stage", respectively.

D Example average traces of ERGs of control animals (left, *nSyb-Gal4*/+), flies with *synj* null mutant eyes (*synj*$^{-/-}$), flies with *synj* null mutant eyes expressing *synj*^{RQ} or *synj*$^{+}$ (*UAS synj*^{RQ}, *synj*$^{-/-}$ and *UAS synj*$^{+}$, *synj*$^{-/-}$), control animals (right, w^{1118}), and *synj*^{RQ} knock-in animals. Full genotypes appear in the Appendix Supplementary Methods. "ON" and "OFF" peaks are indicated with arrowheads. Note that while *synj* null mutants display severe defects in their ERG traces, *synj*^{RQ} mutants do not. $n > 20$ animals per genotype.

E–J Representative images of boutons loaded (1 min, 90 mM KCl) with FM 1-43 (E–I) and quantification (J) of the following genotypes: control (left, *D42-Gal4*/+) (E), *synj* null mutants (*synj*$^{-/-}$) (F), *synj* null mutants that express *synj*^{RQ} (G), or *synj*$^{+}$ (H) (*UAS synj*^{RQ}, *synj*$^{-/-}$ and *UAS synj*$^{+}$, *synj*$^{-/-}$), control animals (right, w^{1118}; image not shown, only quantification is included) and *synj*^{RQ} knock-in animals (I). Full genotypes appear in the Appendix Supplementary Methods. Scale bar, 5 μm. Note that *synj*^{RQ} internalizes as much FM 1-43 as controls do. For UAS experiments, statistical analysis with one-way ANOVA Kruskal–Wallis followed by Dunn's multiple comparison *post hoc* test, ****$P < 0.0001$; ns, not significant; $n \geq 7$ larvae and $n \geq 14$ NMJs per genotype. For *synj*^{RQ} experiment: *t*-test, $P > 0.05$, $n = 10$ larvae and $n = 20$ NMJs per genotype. Error bars represent SEM.

K Quantification of the number of satellite boutons per NMJ of the genotypes in (E–I). Note that while *synj* null mutants harbor numerous satellite boutons, *synj*^{RQ} mutants do not. Statistical analysis for UAS experiments: one-way ANOVA Kruskal–Wallis followed by Dunn's multiple comparison *post hoc* test, *$P < 0.05$, $n \geq 4$ larvae and $n \geq 16$ NMJs per genotype. For *Synj*^{RQ} experiment: *t*-test, $P > 0.05$, $n = 6$ larvae and $n \geq 14$ NMJs. Error bars represent SEM.

L, M Quantification (L) of the EJC amplitude recorded at third-instar larval NMJs of the indicated genotypes (see also E–I) and sample EJC traces (M). Statistical analysis, one-way ANOVA Kruskal–Wallis followed by Dunn's multiple comparison *post hoc* test, $P > 0.05$, $n \geq 8$ larvae per genotype. Error bars represent SEM.

N Cumulative histograms of mEJC amplitudes and sample EJC traces recorded at third-instar larval NMJs of the indicated genotypes (see also E–I). $n \geq 7$ larvae for indicated genotypes.

O, P Relative EJP amplitudes recorded during a 10-min 10-Hz stimulation train of the genotypes indicated in (E–I). Please see Materials and Methods for details. Data for the *synj* null mutants that express *synj*^{RQ} or *synj*$^{+}$ are not significantly different from control (*D42-Gal4*/+), whereas a significant difference is observed from data point 3 till the end of the recording of *synj* null mutants (*synj*$^{-/-}$) compared to control (ns: data points 1–2, *$P < 0.05$: data point 3, **$P < 0.01$: data points 4, 16–21, ***$P < 0.001$: data points 5, 13–15, ****$P < 0.0001$: data points 6–12). Statistical analysis for UAS experiments: one-way ANOVA Kruskal–Wallis followed by Dunn's multiple comparison *post hoc* test, $n \geq 4$ larvae indicated genotypes in (O). Data for *Synj*^{RQ} compared to control are not significantly different. Statistical analysis by *t*-test, $P > 0.05$, and $n \geq 8$ larvae for indicated genotypes in (P). Error bars represent the SEM. Note that *synj* null mutants do not maintain neurotransmitter release whereas the *synj*^{RQ} mutants maintain release similar to controls.

loss significantly reduces FM 1-43 labeling compared to controls (Verstreken *et al*, 2003). This labeling is restored by neuronal expression of wild-type *synj*, and again also by Synj^{RQ} (Fig 1E–H and J). We confirmed that Synj^{RQ} rescues the *synj* knockout phenotype independent of overexpression by finding normal FM 1-43 dye uptake in *synj*^{RQ} knock-in animals (Fig 1I and J). Thus, FM 1-43 labeling suggests that Synj^{RQ} supports presynaptic vesicle recycling and, under the conditions we tested, does so as efficiently as wild-type Synj.

The disruption of NMJ endocytosis often correlates with morphological defects. These also occur in the *synj* null mutants in the form of numerous satellite boutons that are small protrusions emanating from the primary axial branch (Dickman *et al*, 2006). We therefore examined whether Synj^{RQ} possesses sufficient Synj activity to suppress this defect. We find a significant rescue of this *synj* null mutant-associated satellite bouton phenotype in *synj* null mutants that transgenically express wild-type Synj^{+} or mutant Synj^{RQ}. We also observe no difference in satellite bouton number between *synj*^{RQ} knock-in animals and controls (Fig 1K). Hence, Synj^{RQ} appears to allow enough endocytosis to suppress this classic readout of NMJ endocytic defects, and is markedly different to the *synj* null allele.

We next directly examined how well Synj^{RQ} supports neurotransmission at the larval NMJ. First, we measured basal release characteristics including miniature excitatory junctional currents (mEJC) and EJCs. In controls and *synj* null mutants expressing Synj^{+} or Synj^{RQ}, no difference is observed in mEJC and EJC amplitude nor in frequency (Fig 1L–N). We then stimulated the motor nerves for 10 min at 10 Hz to continuously drive synaptic vesicle exo- and endocytosis, and measured the post-synaptic excitatory junctional potentials (EJP). While control NMJs maintain neurotransmitter release under these conditions, *synj* null mutants fail to do so, and the block in endocytosis causes the EJP amplitude to drop to a low level in the first minutes of stimulation (Fig 1O) (Verstreken *et al*, 2003). This neurotransmission defect is rescued by transgenic neuronal expression of wild-type Synj^{+}, or Synj^{RQ} (Fig 1O). Here also, *synj*^{RQ} knock-in animals maintain release during this 10-Hz stimulation train at a level comparable to controls (Fig 1P). Synj^{RQ} was previously shown to lack SAC1 domain phosphatase activity (Krebs *et al*, 2013) and our data now suggest that the Synj^{RQ} mutant protein can support synaptic vesicle cycling. These results are consistent with data obtained in mouse cortical neurons using SAC1-dead Synj1 mutants that also supported vesicle recycling during persistent activity (Mani *et al*, 2007).

Synaptojanin is required for autophagosome formation in presynaptic terminals

Given that Synj is strongly enriched at presynaptic terminals (Verstreken *et al*, 2003), Synj1^{R258Q} lacks PI(3)P phosphatase activity (Krebs *et al*, 2013), and the importance of PI(3)P on autophagosomes (Simonsen & Tooze, 2009; Burman & Ktistakis, 2010; Noda *et al*, 2010; Dall'Armi *et al*, 2013; Devereaux *et al*, 2013), we hypothesized that the Synj SAC1 domain acts in synaptic autophagy. We and others recently showed the presence of autophagic markers at presynaptic terminals (Williamson *et al*, 2010; Hernandez *et al*, 2012; Zhu *et al*, 2013; Maday & Holzbaur, 2014; Wang *et al*, 2015, 2016; Soukup *et al*, 2016; Stavoe *et al*, 2016). To determine whether Synj localizes on autophagic membranes, we examined the interaction between Synj and the transmembrane Atg9 marker of early pre-autophagosomal membranes (He *et al*, 2006; Tamura *et al*, 2010; Yamamoto *et al*, 2012; Stavoe *et al*,

2016). The distribution of a genomic Atg9^{HA} construct where Atg9^{HA} is expressed under endogenous promotor control is broad (Appendix Fig S2A–A″), consistent with the idea that Atg9 decorates early autophagic vesicles and autophagosomes. Next, we used anti-HA to immunoprecipitate neuronal autophagosomal membranes from fly heads expressing Atg9^{HA} at endogenous levels. We detect the co-immunoprecipitation of Synj with the Atg9-positive membrane fraction in both wild-type and *synj*^{RQ} knock-in animals expressing Atg9^{HA} (Fig 2A). In contrast and indicating specificity, other synaptic proteins (alpha-SNAP and complexin) do not co-immunoprecipitate (Fig 2A).

Next, we assessed whether Synj is important for presynaptic autophagy. Such a role had recently been suggested in zebrafish cone photoreceptors (George *et al*, 2016). We expressed transgenes for the Atg8^{mCherry} (fly LC-3) marker of mature autophagosomes (Kabeya *et al*, 2000) and Lamp1^{GFP}, an autolysosomal marker (Marzella *et al*, 1982; Juhász *et al*, 2008), in motor neurons using *D42-Gal4*. In control animals, autophagy induced by starvation (amino acid deprivation) is marked by the presence of punctate dots of Atg8^{mCherry} signal within presynaptic terminals (Fig 2B, B′, and G) that we previously characterized by correlative light and electron microscopy (CLEM) as synaptic autophagosome-like structures (Soukup *et al*, 2016). Moreover, boutons of starved control animals also accumulate the Lamp1^{GFP} marker (Appendix Fig S2B, B′, and F). In contrast, in *synj* null mutants and *synj* null mutants that express Synj^{RQ}, the Atg8^{mCherry} and Lamp1^{GFP} redistribution is blocked (Fig 2C–D′ and G, and Appendix Fig S2C–D′ and F). Unlike our findings with Synj-driven endocytosis, we observe that only wild-type Synj^{+}, and not Synj^{RQ}, can recover the Synj function in presynaptic autophagy (Fig 2F and G, and Appendix Fig S2E and F). Our results are also not unique to "starvation-induced autophagy" because when we induce the process by direct electrical motor neuron stimulation (30 min 20 Hz) (Soukup *et al*, 2016), the clear increase in the number of Atg8 dots observed in controls is absent in *synj*^{RQ} mutants (Fig 2H–J).

To scrutinize our results further and provide evidence that the block in synaptic autophagy is caused by the lack of SAC1 activity, we created flies that express Synj^{C396S} (Synj^{CS}), a SAC1 enzymatic dead mutant (Mani *et al*, 2007). We expressed Synj^{CS} in *synj*$^{-/-}$ null mutants under the same conditions as used to express Synj^{RQ} using *D42-Gal4* driver. We then assessed Atg8^{mCherry} localization and found that Atg8^{mCherry} also does not concentrate in dots upon induction of starvation (Fig 2E, E′, and G). These data are in further support of the notion that Synj SAC1 domain function is required for synaptic autophagy and that the pathogenic PD mutant Synj behaves in this respect similar to a Synj-SAC1 domain mutant.

Next, to distinguish whether loss of Synj SAC1 function blocks autophagosome formation or promotes autophagosome degradation, we pharmacologically blocked the fusion of autophagosomes with late endosomes/lysosomes using chloroquine (Stauber *et al*, 1981; Chi *et al*, 2010). Subsequently, we monitored Atg8^{mCherry} localization. As expected in wild-type controls, chloroquine under fed or starved conditions causes an increase in the number of Atg8^{mCherry} dots. In contrast, in *synj*^{RQ} mutants, chloroquine does not result in such an increase in the number of Atg8^{mCherry} dots (Fig 2K–M), suggesting autophagosome biogenesis is slowed. We provide further evidence for this by using the flux marker Atg8 tagged with GFP and RFP in tandem. Here, Atg8-positive organelles are green and red fluorescent, but when they fuse with lysosomes, the GFP is quenched and autolysosomes are only red (DeVorkin & Gorski, 2014). We quantified the number of yellow and red Atg8-positive organelles in controls as well as the rare Atg8-positive organelles in *synj*^{RQ} mutants. We do not observe a significant difference in the ratio of red (mature) over total Atg8-labeled organelles between control and *synj*^{RQ} (Control: 55%; *synj*^{RQ}: 57%). The data indicate that once a rare Atg8-positive autophagosome manages to form in *synj*^{RQ} mutants, its further maturation is not impeded (Appendix Fig S2G–I).

Synj mutants accumulate Atg18a within synaptic boutons

Members of the PROPPIN domain-containing protein family are key PI(3)P- and PI(3,5)P_2-binding proteins with a role in autophagy (Baskaran *et al*, 2012). Given that Synj1^{RQ} cannot dephosphorylate PI(3)P (and likely PI(3,5)P_2), we hypothesized that in the *synj* null mutants that express Synj^{RQ}, autophagic PROPPIN-containing proteins would accumulate on synaptic pre-autophagosomal membranes. Therefore, we generated flies expressing N-terminal GFP-tagged *Drosophila* homologs of the PROPPIN WIPI2 (Atg18a, Atg18b, and CG11975; 70.8, 56.5, and 32.0% identity to human WIPI2 respectively). Both Atg18a^{GFP} and

Figure 2. Synaptojanin is required for synaptic autophagy.

A Western blot of an anti-HA immunoprecipitation from control fly heads (*w*^{1118}), Atg9^{HA}-expressing fly heads (*w;;Atg9*^{HA}) and *w;synj*^{RQ}*;Atg9*^{HA}. Blots probed with anti-Synj to assess whether Synj (predicted 134 kDa) is present on Atg9-positive structures; anti-HA to assess immunoprecipitation specificity, Atg9^{HA} (predicted 96 kDa). As control alpha-SNAP (33 kDa) and complexin (cpx; 18 kDa) where probed. Experiments were performed in independent duplicates.

B–G Live imaging of fed (B–F) and 4-h-starved (B′–F′) NMJ boutons of control (*D42-Gal4* > Atg8^{mCherry}) (B, B′) and *synj*$^{-/-}$ null mutants (C, C′) either expressing *synj*^{RQ} (D, D′) or *synj*^{CS} (E, E′) or *synj*$^{+}$ (F, F′) and also expressing Atg8^{mCherry} (*D42-Gal4* > Atg8^{mCherry}). Full genotypes are included in the Appendix Supplementary Methods section. Quantification of the number of Atg8^{mCherry} dots (arrowheads) (G). Statistical analysis with one-way ANOVA Kruskal–Wallis followed by Dunn's multiple comparison *post hoc* test, ****$P < 0.0001$, ***$P < 0.001$, and each genotype individually fed and starved by *t*-test, ****$P < 0.0001$, $n \geq 9$ larvae and $n \geq 18$ NMJs per genotype. Error bars represent SEM; scale bar, 5 μm. Note that loss of Synj blocks the formation of Atg8^{mCherry} dots and this is not rescued by expression of *synj*^{RQ} nor *synj*^{CS}.

H–J Live Atg8^{mCherry} imaging following 30 min of 20-Hz electrical nerve stimulation of indicated genotypes (H, I). Full genotypes are included in the Appendix Supplementary Methods. Quantification of Atg8^{mCherry} dots (arrowheads) (J). Statistical analysis by *t*-test, **$P < 0.01$, $n \geq 8$ larvae and $n \geq 33$ NMJs per genotype. Error bars represent SEM; scale bar, 5 μm.

K–M Images of NMJ boutons of *synj*$^{-/-}$ null mutants either expressing *synj*$^{+}$ (K) or *synj*^{RQ} (L) and also expressing Atg8^{mCherry} (*D42-Gal4* > *Atg8*^{mCherry}) fed (data from G) and fed or starved for 4 h with chloroquine and labeled with anti-mCherry antibodies. Quantification of the number of Atg8^{mCherry} dots (arrows) of indicated genotypes (in detail in the Appendix Supplementary Methods) (M). Statistical analysis by *t*-test, ****$P < 0.0001$, **$P < 0.01$, $n \geq 9$ larvae and $n \geq 18$ NMJs per genotype. Error bars represent SEM; scale bar. 5 μm. Despite that chloroquine blocks autophagosome to lysosome fusion, Atg8^{mCherry} dots still do not form in animals expressing *synj*^{RQ}.

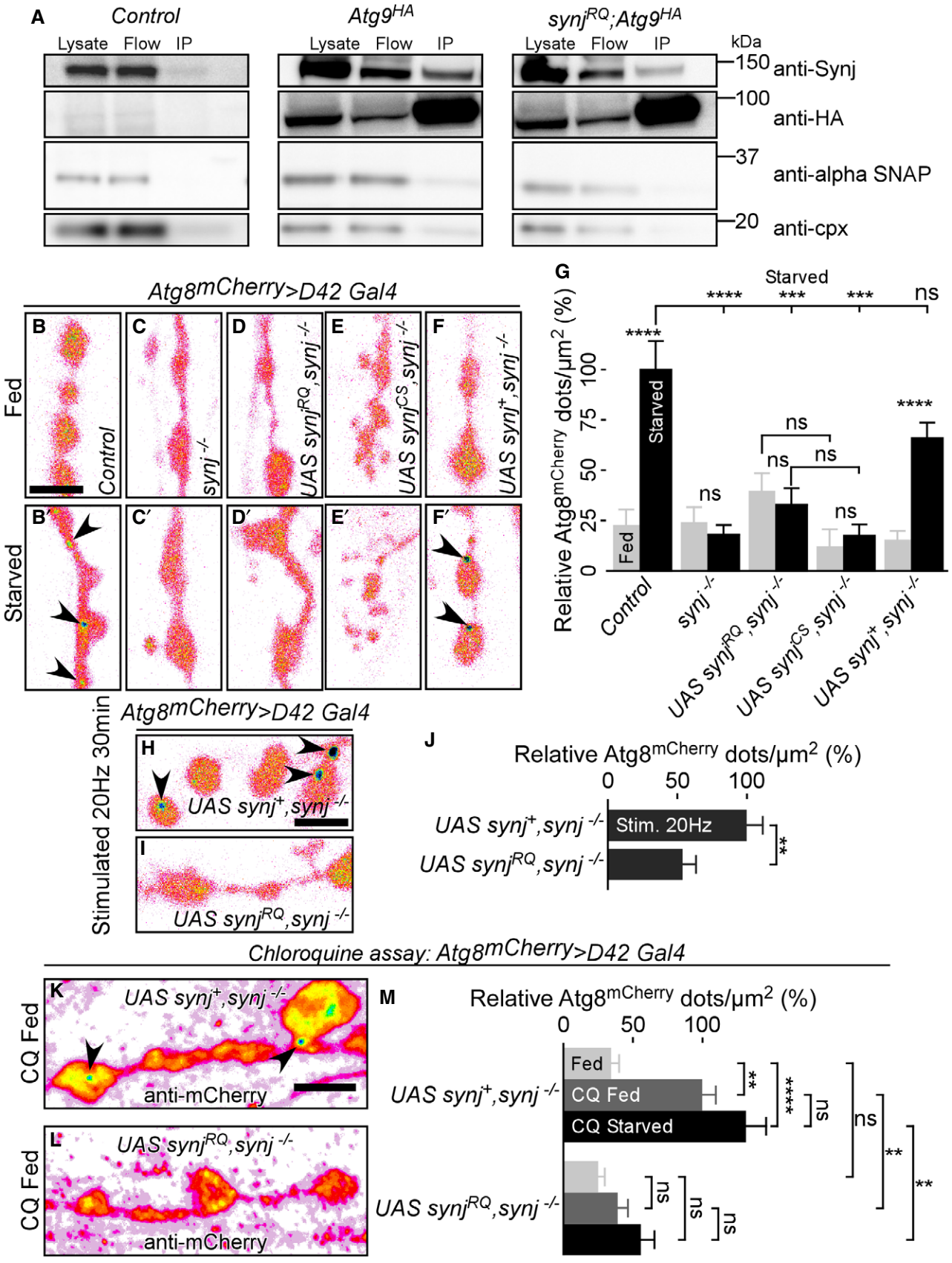
A
Control
Atg9HA
synjRQ;Atg9HA
Lysate Flow IP
kDa
150
100
37
20
anti-Synj
anti-HA
anti-alpha SNAP
anti-cpx
Atg8mCherry>D42 Gal4
Fed
Starved
Control
synj -/-
UAS synjRQ,synj -/-
UAS synjCS,synj -/-
UAS synj+,synj -/-
G
Starved
Relative Atg8mCherry dots/µm2 (%)
Fed
Stimulated 20Hz 30min
UAS synj+,synj -/-
UAS synjRQ,synj -/-
J
Stim. 20Hz
Chloroquine assay: Atg8mCherry>D42 Gal4
CQ Fed
anti-mCherry
M
CQ Starved
ns

Figure 2.

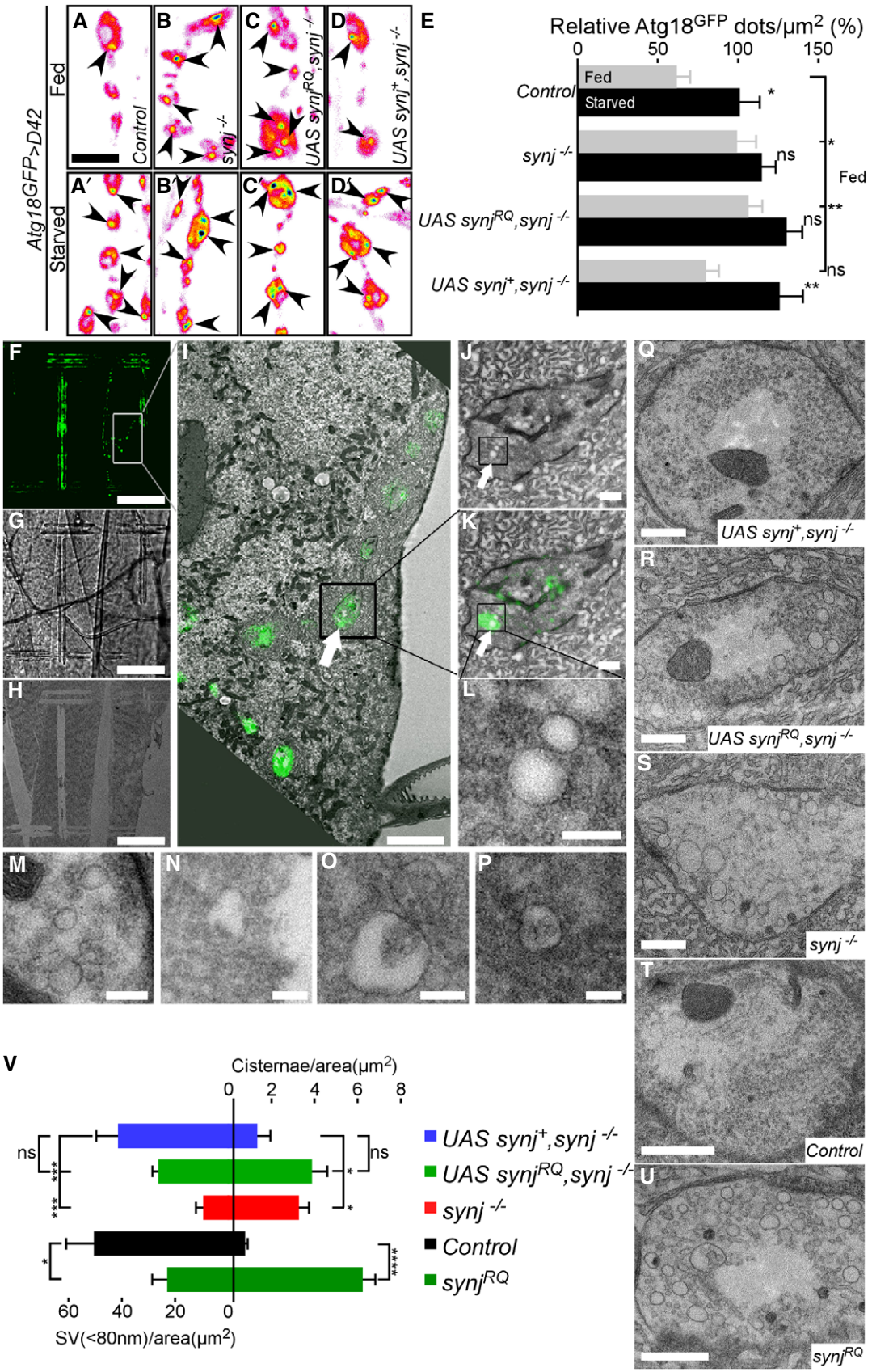

Figure 3.

CG11975^{GFP} localize in puncta at synaptic boutons when expressed in motor neurons (*D42-Gal4*) (Appendix Fig S3A, B, G, and H). In contrast, Atg18b^{GFP} is retained in neuronal cell bodies (Appendix Fig S3E and F). After starvation, we observe a clear upregulation of the number of Atg18a^{GFP} puncta, while the number of CG11975^{GFP} dots does not change (Appendix Fig S3C, D, I, and J and Fig 3A, A′, and E). Additionally, Atg18a^{GFP} puncta sometimes colocalize with Atg8^{mCherry} puncta (Appendix Fig S3K and L) and expression of Atg18a^{GFP} using the ubiquitous *Da-Gal4* driver in *atg18a* null mutants rescues their lethality. These data indicate that Atg18a^{GFP} is a functional protein.

We then assessed Atg18a^{GFP} localization in *synj* null mutants that express *synj^{RQ}*. Consistent with Synj^{RQ} not being able to dephosphorylate PI(3)P (Krebs *et al*, 2013), we find a significant increase in the number of Atg18a^{GFP} dots in fed *synj* mutants in comparison with fed controls (Fig 3A–C′ and E). In addition, the number of Atg18a^{GFP} dots is also increased in *synj* null mutant boutons that express *synj^{RQ}* compared to *synj* null mutant boutons that express *synj^{+}* (Fig 3C–E). Atg18a can bind PI(3)P and PI(3,5)P_2 that are both dephosphorylated by the SAC1 domain of Synj1. To delineate which phosphoinositide is involved, we took a pharmacological approach. We used wortmannin (WM) that inhibits Vps34, a kinase that produces PI(3)P, or YM201636 (YM) that inhibits PIKfyve, a kinase that produces PI(3,5)P_2. We applied these drugs during starvation to control and *synj^{RQ}* mutant animals that express Atg18a^{GFP}. While Atg18a^{GFP} accumulates in dots in starved controls, application of either drug blocks this effect and Atg18a^{GFP} does not accumulate anymore, indicating that Atg18a^{GFP} likely binds both PI(3)P and PI(3,5)P_2 during autophagy at synapses (Appendix Fig S3M). In *synj^{RQ}* mutants, the number of Atg18a^{GFP} dots is always upregulated. However, when we starve the larvae in the presence of either WM or YM, the number of Atg18a^{GFP} is lower than in untreated starved *synj^{RQ}* mutants (Appendix Fig S3M). These data suggest that consistent with the previously established function of the Synj SAC1 domain, both PI(3)P and PI(3,5)P_2 accumulate and bind Atg18a in *synj^{RQ}* mutants.

We tried to find further evidence for upregulation of PI(3)P in *synj^{RQ}* using expression of 2xFYVE-GFP, a probe that binds PI(3)P. We were however unsuccessful and did not detect obvious differences (not shown). Nonetheless, we do believe our results are consistent with the specific loss of SAC1 domain function in *synj^{RQ}*. We assessed 5-phosphatase domain activity of Synj using the PLCδ-PH-eGFP probe that detects PI(4,5)P_2. We find that the synaptic labeling intensity of PLCδ-PH-eGFP is much less affected in *synj* null mutants that express Synj^{RQ} (where 5-phosphatase activity is not affected) compared to *synj* null mutants (where 5-phosphatase activity is affected) (Appendix Fig S3N–R), suggesting *synj^{RQ}* mutants support PI(4,5)P_2 dephosphorylation. Taken together, the data are consistent with normal PI(4,5)P_2 dephosphorylation activity of Synj1^{RQ} measured *in vitro* (Krebs *et al*, 2013), but altered PI(3)P dephosphorylation, thereby leading to the accumulation of Atg18a at synaptic boutons in *synj^{RQ}* mutants.

Visualization of Atg18a-labeled structures at synaptic boutons

Synapses in *synj* mutants expressing Synj^{RQ} harbor increased synaptic Atg18a^{GFP} accumulations and largely lack Atg8^{mCherry} accumulations. To further visualize the Atg18a^{GFP}-labeled structures, we resorted to CLEM, a methodology that allows us to directly determine the ultrastructural appearance of Atg18a-positive structures within synaptic boutons. *Synj* mutants expressing Synj^{RQ} and Atg18a^{GFP} were dissected, fixed, and imaged. Subsequently, a near-infrared laser was used to produce burn marks in the vicinity of the imaged region. These marks are easily discernable at the light and EM level and help us when producing serial sections of the imaged boutons (Fig 3F–H). After alignment of the confocal images with the serial TEM images, we are able to identify the Atg18a^{GFP}-positive structures (Fig 3I–K). As indicated in Fig 3L–P, Atg18a^{GFP} marks profiles that have the appearance of cisternae that sometimes contain a few smaller vesicular structures in their lumen. Given that the flux of synaptic autophagy is blocked in *synj* mutants expressing Synj^{RQ} and that these mutants do not harbor Atg8^{mCherry} dots, we

Figure 3. Atg18a-positive structures accumulate at synaptic boutons of *synj* mutants.

A–E Live imaging of fed (A–D) and 4-h-starved (A′–D′) NMJ boutons in controls (*D42-Gal4* > Atg18a^{GFP}) (A, A′) and *synj$^{-/-}$* null mutants (B, B′) or *synj$^{-/-}$* null mutants expressing either *synj^{RQ}* (C, C′) or *synj^{+}* (D, D′) and also expressing Atg18a^{GFP} (*D42-Gal4* > Atg18a^{GFP}). Quantification of the number of Atg18a^{GFP} dots (arrowheads) of indicated genotypes under fed and starved conditions (E). Full genotypes appear in the Appendix Supplementary Methods. Statistical analysis by *t*-test comparing control to individual genotypes separately in fed conditions and each genotype individually fed and starved, $^{**}P < 0.01$, $^{*}P < 0.05$, $n \geq 10$ larvae and $n \geq 20$ NMJs per genotype. Error bars represent SEM; scale bar, 5 μm. Note that loss of Synj increases the number of Atg18a^{GFP} dots even under fed conditions. This is not rescued by expression of *synj^{RQ}*.

F–P Correlative light and electron microscopy (CLEM) of 4-h-starved *synj$^{-/-}$* null mutant NMJ boutons expressing Atg18a^{GFP} and *synj^{RQ}* under the control of *D42-Gal4*. NMJ boutons with Atg18^{GFP} fluorescence were imaged (F), and subsequently surrounded by burn marks using near-infrared branding (NIRB) (F–H). Branding marks are clearly visible in transmission and fluorescent mode due to autofluorescence of the marks (F, G). Branding marks allow subsequent detection of the same region of interest in electron micrographs (H). The marks then allow for the correlation of fluorescent and electron micrographs of Atg18a^{GFP}-positive boutons (I–K). Arrows indicate Atg18^{GFP}-positive labeling (intensities were adjusted as to identify structures) in EM micrographs and boxes are enlarged in subsequent panels. Magnification of Atg18a^{GFP}-positive structures identified in (I–K) is shown in (L) and further examples of Atg18^{GFP}-labeled structures are taken from independent CLEM experiments (M–P). Scale bars: 50 μm (F–H), 5 μm (I), 50 nm (J, K), and 200 nm (L–P).

Q–U Representative transmission electron micrographs of 4-h-starved *synj$^{-/-}$* null mutants expressing either *synj^{+}* (Q) or *synj^{RQ}* (R) using *D42-Gal4*, as well as of 4-h-starved *synj$^{-/-}$* null mutants (S), controls (*w^{1118}* (T)), and *synj^{RQ}* knock-in animals (U). Full genotypes appear in the Appendix Supplementary Methods. Scale bars, 1 μm.

V Quantification of the number of synaptic vesicles (diameter < 80 nm) and cisternae that resemble Atg18a^{GFP}-positive structures identified using CLEM. Note that at boutons of *synj$^{-/-}$* null mutants, *synj$^{-/-}$* null mutants expressing *synj^{RQ}* and *synj^{RQ}*, there are cisternae that resemble the Atg18a^{GFP}-positive structures identified in CLEM; in *synj$^{-/-}$* null mutants expressing *synj^{RQ}* and in *synj^{RQ}* knock-in, there are numerous synaptic vesicles detectable. For statistical analysis of both SV and cisternae, *t*-test comparing genotypes individually, $^{*}P < 0.05$, $^{***}P < 0.001$, $^{****}P < 0.0001$. $n \geq 3$ larvae and $n \geq 8$ NMJs per genotype. Error bars represent SEM.

propose that these cisternae are early presynaptic autophagic intermediates.

Using the morphological features of Atg18a^{GFP}-positive structures as a guide, we assessed the ultrastructural morphology of synapses in starved animals. We used TEM images to quantify the number of synaptic vesicles and the number of structures that have an appearance similar to the Atg18a-positive cisternae in our CLEM studies (Fig 3V). Compared to starved controls and *synj* null mutants expressing Synj$^+$, starved *synj* null mutants show a strong reduction in the number of synaptic vesicles per bouton area, consistent with a defect in synaptic endocytosis. These mutants also show an increased number of cisternal structures (Fig 3Q, S, T, and V), correlating with an increased number of Atg18a-positive dots in *synj* null mutants. Starved *synj* null mutants that express *synj*^{RQ} and *synj*^{RQ} knock-in animals also show an increased number of cisternal structures at boutons (Fig 3R, U, and V). However, there is a largely normal number of synaptic vesicles compared to controls (Fig 3Q–V), consistent with the normal synaptic vesicle endocytosis that we measured in these mutants (see Fig 1).

Synaptojanin regulates Atg18a mobility at autophagosomal membranes

In synaptic vesicle endocytosis, the dephosphorylation of PI(4,5)P_2 by Synj on nascent vesicles regulates the detachment of adaptors with affinity for this lipid. We reasoned that a similar mechanism may be at play during autophagosome formation and tested whether Synj regulates Atg18a attachment and detachment. We expressed Atg18a^{GFP} and assessed the fluorescence recovery after bleaching one specific Atg18a^{GFP} dot. *Synj* null mutants and *synj* null mutants expressing Synj^{RQ} show significantly slower recovery of Atg18a fluorescence in the bleached area compared to *synj* null mutants expressing Synj$^+$ or compared to wild-type controls (Fig 4A–E).

To find further evidence for our model, we also generated Atg18a$^{mEOS3.2}$-expressing flies. mEos is a photoconvertible fluorescent protein that shifts from green to red fluorescence when activated (Zhang *et al*, 2012). We reasoned that Atg18a mobility would decrease after induction of autophagy, as more Atg18a would bind to newly forming autophagosomes. Therefore, we used single-particle tracking photoactivation localization (sptPALM) microscopy to track single molecules within synaptic boutons expressing Atg18a$^{mEOS3.2}$ (Bademosi *et al*, 2017). Tracking each fluorescent molecule (Video EV1) allows us to generate trajectory maps of Atg18a$^{mEOS3.2}$, as well as intensity and instantaneous diffusion coefficient maps (Fig 4F–F‴). Moreover, we quantified Atg18a$^{mEOS3.2}$ mobility by analyzing the mean square displacement (MSD) of sptPALM trajectories of single fluorescent localizations (Fig 4G). Compared to fed larvae, Atg18a mobility significantly decreases in starved larvae (Fig 4H), in good agreement with recruitment of cytosolic molecules to presynaptic autophagosomes. Analysis of the diffusion coefficient distribution reveals a decrease in the mobile population of Atg18a$^{mEOS3.2}$ in starved conditions (Fig 4I). This is most apparent in the ratio of the mobile-to-immobile fractions (Fig 4J). This change in mobility of Atg18a after induction of autophagy is consistent with the recruitment of Atg18a to presynaptic autophagosomes.

We subsequently followed the accumulation of Atg18a on synaptic autophagosomes by converting a boutonic pool of Atg18a$^{mEOS3.2}$. We converted Atg18a$^{mEOS3.2}$ in one bouton and followed accumulation of red Atg18a$^{mEOS3.2}$ on (green Atg18a$^{mEOS3.2}$-positive) autophagosomes in the neighboring boutons of control and *synj*^{RQ} knock-in flies. While the amount of red photoconverted Atg18a in the cytoplasm of controls and *synj*^{RQ} is similar, the red Atg18a accumulates significantly less quickly on nascent autophagosomes in *synj*^{RQ} compared to controls (Fig 4K–M). This slowed acquisition of red fluorescence indicates reduced exchange between membrane bound and soluble pools of Atg18a, and thus indicates that the SAC1 domain of Synj normally promotes Atg18a mobility at synaptic autophagosomes.

Synj^{RQ} reduces lifespan upon starvation and causes neurodegeneration

To more broadly assess the physiological consequences of the Synj^{RQ} mutation, we examined whether this affects animal survival under starvation conditions, a readout that is strongly modulated by autophagy (Juhász *et al*, 2007). While wild-type flies reared in these conditions can survive for ~4 days, we detect significantly reduced survival times for *synj* null mutants that

Figure 4. Synaptojanin regulates Atg18a uncoating at autophagosomal membranes.

A–E Representative time-lapse images of a FRAP experiment where the fluorescence recovery after bleaching of an individual Atg18a^{GFP} dot (*D42-Gal4* > Atg18a^{GFP}) was monitored at a synaptic bouton of a control (A) and of a *synj*$^{-/-}$ null mutant (B) and of a *synj*$^{-/-}$ null mutant expressing either *synj*^{RQ} (C) or *synj*$^+$ (D) (expressed using the *D42-Gal4*). (E) Quantification of fluorescence intensities of a bleached Atg18a^{GFP} dot (arrowheads) in the indicated genotypes (in % of initial fluorescence of the Atg18a^{GFP} dot before bleaching), error bars represent SEM. Full genotypes appear in the Appendix Supplementary Methods. Note the reduced fluorescence recovery of Atg18a in *synj* null mutants and *synj* null mutants expressing *synj*^{RQ} compared to wild-type controls. Even in wild-type Atg18a^{GFP}, fluorescence never recovers more than 60%, suggesting an immobile pool of protein on the nascent autophagosome.

F–J Transgenic larvae expressing Atg18a$^{mEos3.2}$ were imaged at 33 Hz. (F–F‴) Representative low-resolution image of NMJ bouton (F), sptPALM trajectory map (F′), average intensity (F″), and diffusion coefficient (F‴) of Atg18a$^{mEos3.2}$. Scale bar, 5 μm. (G) Comparison of MSD of Atg18a$^{mEos3.2}$ in fed and starved conditions ($n \geq 6$ larvae and $n \geq 18$ NMJ per condition). (H) Analysis of the area under the MSD curve (μm^{2}s) showed significant decrease in starved compared to fed controls. (I) Diffusion coefficient distribution of Atg18a$^{mEos3.2}$ in fed and starved controls. (J) Mobile-to-immobile ratio for fed (13.4 ± 1.8) significantly reduced in starved conditions (7.1 ± 0.5). Statistical analysis by one-way ANOVA with Tukey's multiple comparison test, $^{**}P < 0.01$. Error bars represent SEM.

K–M Representative time-lapse images of mEOS3.2 photoconversion experiment were the RFP fluorescence recovery on an individual Atg18a$^{mEOS3.2}$ after GFP conversion of the neighboring bouton, an individual Atg18a$^{mEOS3.2}$ dot (*D42-Gal4* > Atg18a$^{mEOS3.2}$) was monitored at a synaptic bouton of a control (K) and of a *synj*^{RQ} (L). (M) Quantification of the ratio RFP/GFP fluorescence intensities of an Atg18a$^{mEOS3.2}$ dot (arrowheads) in the indicated genotypes (in % of final time point (10 min after photoconversion) RFP/GFP fluorescence ratio of the Atg18a$^{mEOS3.2}$ dot), error bars represent SEM. Full genotypes appear in the Appendix Supplementary Methods. Statistical analysis comparing curves fitted by linear regression. $n \geq 3$ larvae and $n \geq 13$ NMJs per genotype. Note the reduced RFP/GFP fluorescence recovery of Atg18a$^{mEOS3.2}$ in *synj*^{RQ} compared to wild-type controls.

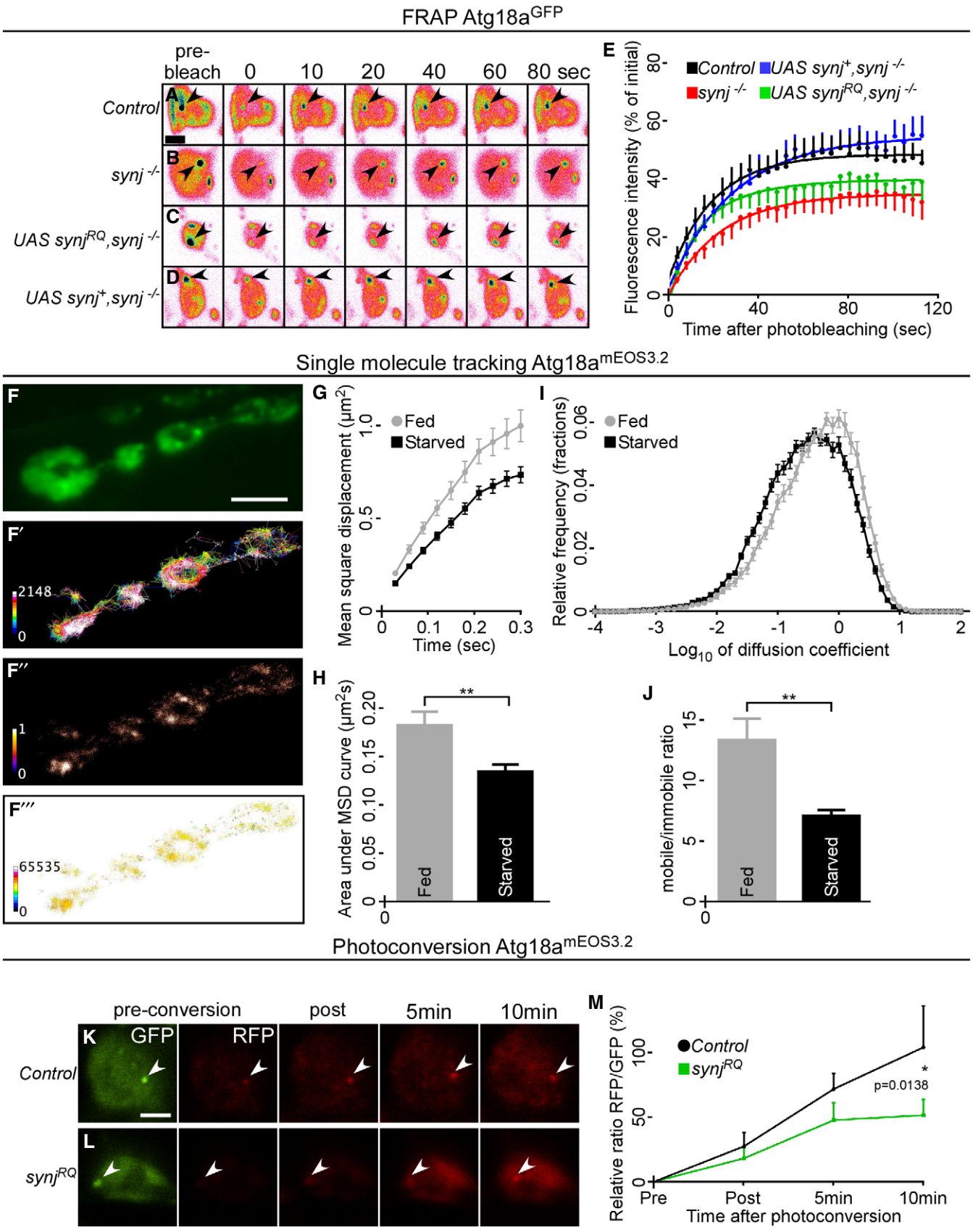
FRAP Atg18a^GFP
pre-bleach
0
10
20
40
60
80 sec
Control
synj -/-
UAS synj^RQ,synj -/-
UAS synj+,synj -/-
A
B
C
D
E
Control
UAS synj+,synj -/-
synj -/-
UAS synj^RQ,synj -/-
Fluorescence intensity (% of initial)
Time after photobleaching (sec)
Single molecule tracking Atg18a^mEOS3.2
F
F′
F″
F‴
2148
0
1
65535
G
Fed
Starved
Mean square displacement (µm²)
Time (sec)
I
Relative frequency (fractions)
Log10 of diffusion coefficient
H
Area under MSD curve (µm²s)
**
J
mobile/immobile ratio
Photoconversion Atg18a^mEOS3.2
pre-conversion
post
5min
10min
K
GFP
RFP
L
synj^RQ
M
Relative ratio RFP/GFP (%)
p=0.0138
Pre
Post
5min
10min
Time after photoconversion

Figure 4.

express Synj^{RQ} in neurons or *synj*^{RQ} knock-in animals which display 100% lethality within 3 days (Fig 5A and A′). The results correlate with impaired autophagosome maturation in animals lacking Synj SAC1 activity, suggesting that presynaptic autophagy connects to an important survival mechanism during starvation in the fruit fly.

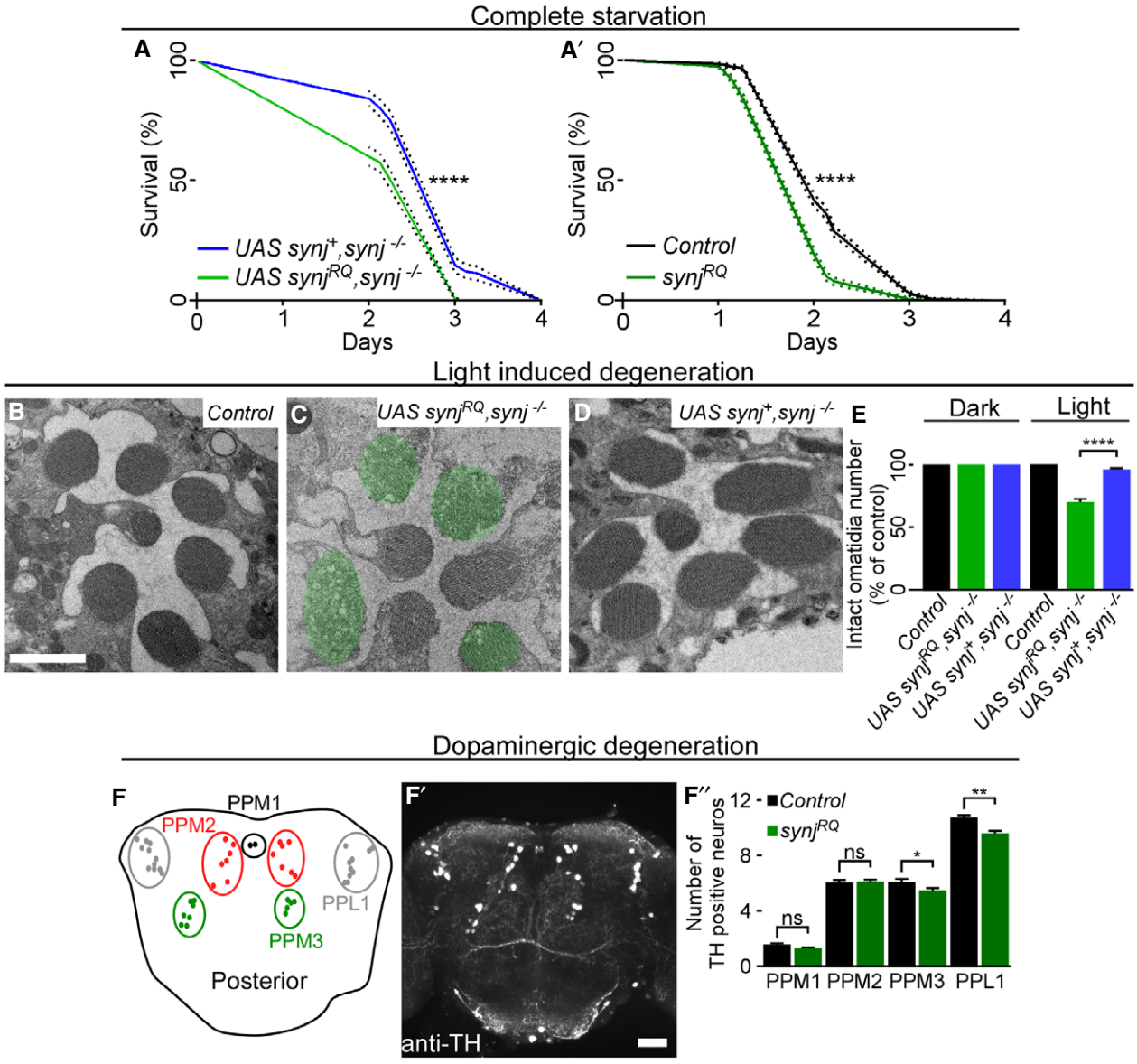

Figure 5. Defects in synaptic autophagy result in reduced lifespan upon starvation and neurodegeneration.

A, A′ Complete starvation (water-only diet) assay in *synj* null mutants expressing *synj*^{RQ} (light green) or *synj*$^{+}$ (blue) (expressed using *nSyb-Gal4*) (A) and *synj*^{RQ} knock-in animals (dark green) as well as controls (w^{1118}, black) (A′). Statistical analysis of survival curves by log-rank (Mantel–Cox) test, ****$P < 0.0001$, $n \geq 134$ flies per genotype for (A) and $n \geq 292$ flies per genotype for (A′), dotted lines surrounding the curves indicate SEM. Note, *synj* null mutants expressing *synj*^{RQ} as well as *synj*^{RQ} knock-in flies have a shorter life span under these starvation conditions.

B–E Representative electron micrographs of the retina after 7 days of continuous light exposure of control (*nSyb-Gal4*/+) (B) and *synj* null mutants expressing *synj*^{RQ} (C) or *synj*$^{+}$ (D) (expressed using *nSyb-Gal4*). Green highlighting in (C) shows disintegrating rhabdomeres as a sign of degeneration. Scale bar, 2 μm. (E) Quantification of number of intact ommatidia per indicated genotype when flies were kept in complete darkness or when exposed to light. Full genotypes are in the Appendix Supplementary Methods. Statistical analysis by *t*-test, ****$P < 0.0001$, n = 3–5 flies per genotype. Error bars represent SEM.

F–F″ Dopaminergic neuron degeneration assay in 30-day-old control (w^{1118}) and *synj*^{RQ} knock-in flies. Schematic representation (F) and image (*z*-stack, sum of slices) of posterior side of an anti-TH-labeled 30-day-old adult fly brain (F′) to show the location of the different dopaminergic neuron cell bodies in this part of the brain. Scale bar, 40 μm. (F″) Bar graph showing the number of dopaminergic neurons (TH-positive) in each cluster indicated in (F) in 30-day-old flies of control (black bars) and *synj*^{RQ} knock-in (dark green bars) flies. Statistical analysis per dopaminergic cluster by *t*-test, **$P < 0.01$, *$P < 0.05$, $n \geq 15$ brains per genotype. Error bars represent SEM. Note at PPM3 and PPL1 dopaminergic neuron clusters the reduction of anti-TH-positive neuronal cell bodies in the of *synj*^{RQ} mutant animals compared to controls.

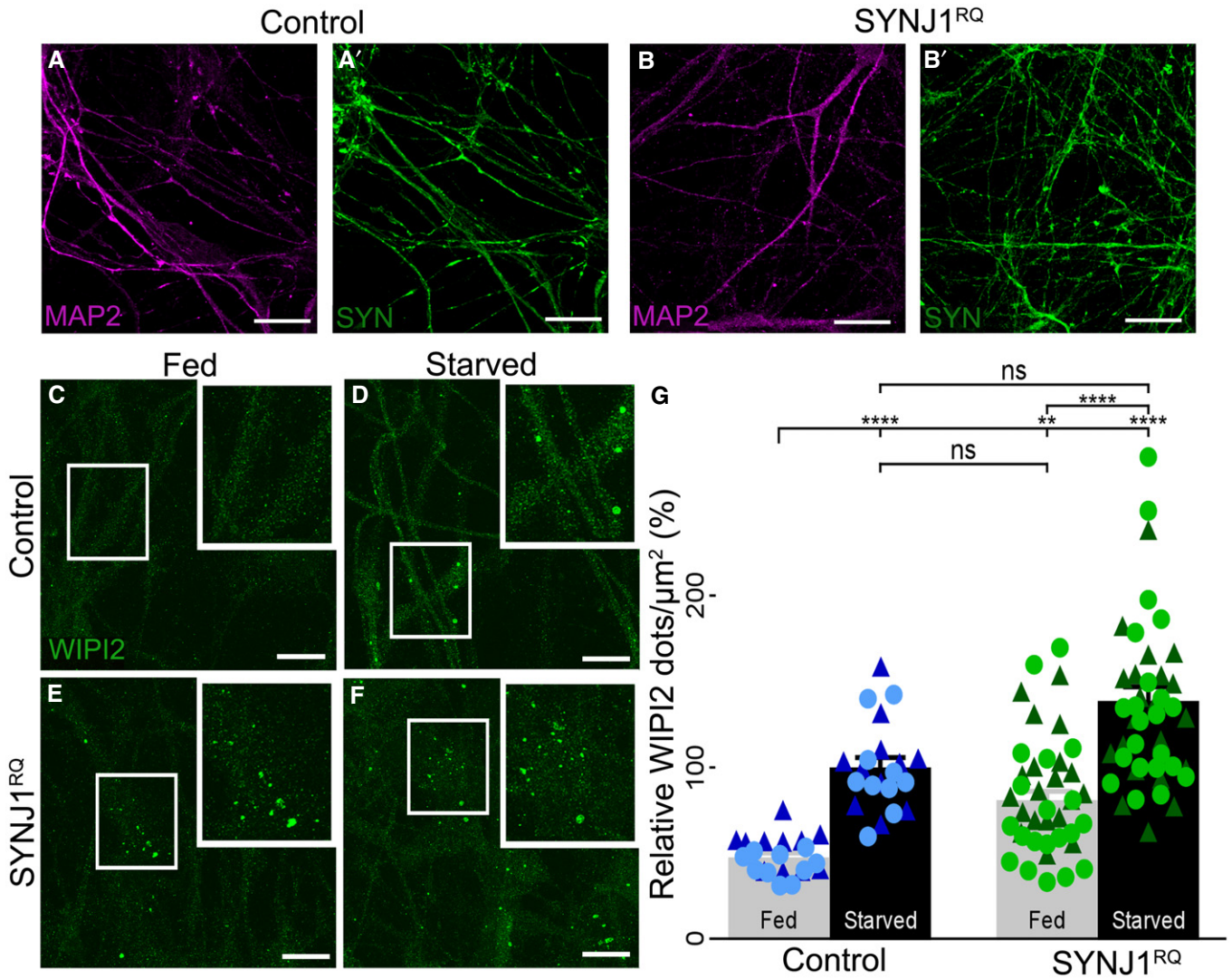

Figure 6. WIPI2/Atg18a accumulates in neurites of *SYNJ1* R258Q human patient iPSC-derived neurons.

A–B′ Immunocytochemistry analysis of human iPSC-derived neurons (after 28 days of differentiation) showing expression of neuronal markers, anti-MAP2 (magenta) and anti-synapsin 1 (green) in control (A, A′) and *SYNJ1*^{RQ} (B, B′). Scale bars, 15 µm.

C–G Images of neurons stained with anti-WIPI2 in fed and starved conditions of controls (C, D) and *SYNJ1*^{R258Q} (E, F). (G) Quantification of the number of WIPI2 dots of indicated genotypes (two control lines and two patients lines (NAPO16 and 17), circles and triangles indicate separate lines for each genotype) under fed and starved conditions. Statistical analysis with one-way ANOVA Kruskal–Wallis followed by Dunn's multiple comparison *post hoc* test, ****$P < 0.0001$, **$P < 0.01$, ns, not significant. $n \geq 21$ images per condition per genotype. Error bars represent SEM; scale bar, 15 µm. Note that SYNJ1^{RQ} has increased number of WIPI2 dots under fed conditions.

Next, we tested neuronal survival, another parameter sensitive to autophagy (Komatsu *et al*, 2006; Juhász *et al*, 2007). To induce neurodegeneration, flies were kept 7 days in constant light challenging photoreceptor neurons of the fly eye. In *synj* null mutant flies that express Synj^{RQ}, a significant reduction in the number of intact ommatidia and an accumulation of vacuoles was observed. In contrast to control animals, when *synj* null mutant animals expressing Synj^{+} or animals kept in dark for 7 days, these photoreceptors appear unaffected (Fig 5B–E). Finally, given the vulnerability of dopaminergic neurons in PD, we assessed the integrity of such neurons in fly brains of 30-day-old *synj*^{RQ} knock-in animals using anti-TH labeling. In these mutants, anti-TH-positive neuronal cell bodies in the PPM3 and PPL1 dopaminergic neuron clusters were significantly reduced compared to controls (Fig 5F–F″). Hence, Synj SAC1 domain function is required for dopaminergic neuron survival in the fly brain.

WIPI2/Atg18a accumulates in neurites of *SYNJ1* R258Q patient-derived human induced neurons

To confirm our key findings in a disease-relevant condition, we resorted to human iPSC obtained from two patients with autosomal recessive, early-onset PD carrying the R258Q mutation in *SYNJ1* as well as two age-matched controls (Appendix Table S1). Following

validation, including expression analysis of pluripotency and proliferation markers (Fig 6A–B′, Appendix Fig S4 and Appendix Table S1), we differentiated these iPSC into neurons. After 28 days of differentiation, we labeled the neurons with anti-WIPI2 (mammalian Atg18a) and imaged the neurites (Fig 6C–F). Similar to our observations at fly synapses, we find a significant increase in the number of WIPI2 dots in starved control neurons compared to fed control neurons (Fig 6C, D, and G). Moreover, in line with our observations made with fly *synj*^{RQ} mutants, we find a significant increase in the number of WIPI2 dots in fed *SYNJ1*^{RQ} neurons compared to fed controls and which is even further increased in starved *SYNJ1*^{RQ} neurons (Fig 6C and E–G). These data indicate that also in human neurons, Synj1 is required for autophagy, and further supports our model that implicates SYNJ1-SAC1 function in removing Atg18a/WIPI2 from nascent autophagosomal membranes.

Discussion

The presynaptic protein SYNJ1 contains two PtdInsP lipid phosphatase domains and is critical for neurotransmission. In this work, we take advantage of both flies and human iPSC-derived neurons obtained from patients carrying the *SYNJ1* R258Q mutation to examine the role of the Synj SAC1 phosphatase domain that is mutated in early-onset PD and that was previously shown to block PI(3)P dephosphorylation (Krebs *et al*, 2013). We show that Synj has a previously unrecognized role in promoting autophagosome maturation within presynaptic terminals and that this is distinct to the relatively well-described function in synaptic vesicle recycling. This predicts that defective synaptic autophagy and protein clearance contributes to *SYNJ1*-PD pathology. Furthermore, given that Synj is a presynaptic protein, these data show the existence of a synapse-specific autophagy machinery and suggest this process may be disrupted in PD.

We detected that Synj has dual presynaptic functions in endocytosis and macroautophagy when comparing the impact of the SAC1-domain mutation and a null mutation. While the *Synj* null mutation causes larval lethality, *Synj*^{RQ} knock-in animals or *synj* null mutants that neuronally express Synj^{RQ} are viable. Similarly, synaptic endocytic mutants cause lethality in flies, while many of the mutants that disrupt macroautophagy are viable (Verstreken *et al*, 2002, 2003; Juhász *et al*, 2007; Soukup *et al*, 2016). Hence, our observation that *synj*^{RQ} flies live is in line with the mutation not disrupting endocytosis. Furthermore, we provide several additional lines of evidence that *Synj*^{RQ} mutants have largely normal synaptic endocytosis. First, Synj^{RQ} mutants have a largely normal number of synaptic vesicles. Second, they display normal presynaptic FM1-43 dye uptake at NMJs. Third, they do not develop the NMJ morphological defects associated with impaired endocytosis. Fourth, we directly assessed how the SAC1 domain *synj*^{RQ} PD mutation affects neurotransmission. Unlike endocytic mutants, we find that the Synj^{RQ} mutant protein maintains NMJ neurotransmitter release during intense stimulation, as well as during normal neurotransmission between the fly eye and brain. These results all indicate that the Synj^{RQ} protein can fulfill the endocytic function of Synj that is required for efficient synaptic vesicle cycling and is severely abnormal in *synj* null animals. Nevertheless, the RQ mutation in *Synj* does incapacitate aspects of Synj activity, as evidenced by loss of dopaminergic neurons and shorter lifespan of *Synj*^{RQ}-expressing flies under starved conditions. We also find that synaptic boutons expressing Synj^{RQ} fail to organize autophagy at presynaptic terminals. Instead, these boutons contain membrane structures positive for the early autophagosome marker Atg18a. Thus, given that under the used conditions, we see that *synj*^{RQ} animals have severely abnormal autophagy alongside normal endocytosis, we conclude that Synj operates in both processes.

Our findings implicate Synj in autophagy at presynaptic terminals, which is surprising given the well-studied role of this protein at the synapse (McPherson *et al*, 1996; Cremona *et al*, 1999; Harris *et al*, 2000; Verstreken *et al*, 2003). We therefore hypothesize that the severe endocytic defects that occur upon *synj* loss made it difficult to detect the importance in autophagy. The conclusion that Synj1 is a dual endocytic and autophagic protein is consistent with the evolutionarily conserved presence of two distinct Synj PtdInsP phosphatase domains, SAC1 and 5-phosphatase, that have different preferences for PtdInsP species. This suggests a cooperativity between the domains and it is interesting to consider the possibility that the dual roles of Synj allow this protein to couple autophagy to levels of synaptic vesicle cycling and thus ensure sufficient protein turnover possibly depending on the level of synaptic activity.

We provide evidence that SAC1-dependent PI(3)P and PI(3,5)P_2 dephosphorylation is needed for normal autophagic flux at synapses using both *Synj*^{RQ} and *Synj*^{CS}, in line with the activities of the PI(3)P phosphatases Ymr1, INP52, and INP53 in yeast cells (Parrish *et al*, 2004). These data in yeast and flies appear at odds with a study in zebrafish where expression of the SAC1 Synj^{C385S} mutant results in a mild and partial rescue of autophagy in cone photoreceptors. While we currently do not understand the nature of this partial rescue, cone photoreceptors are tonically firing neurons (Van Epps *et al*, 2001; Heidelberger *et al*, 2005) and these cells may have different requirements for Synj activity than the spiking neurons at the fly NMJ or mouse hippocampal neurons. Nonetheless, the nature of the partial rescue of autophagy defects upon expression of Synj^{C385S} in zebrafish suggests optimal SAC1 function is needed for normal autophagy. It will be interesting in this context to assess the effect of the Synj Parkinson mutations in zebrafish as well.

While our data indicate an important role of the Synj SAC1 domain in synaptic autophagy, our data do not exclude that the Synj 5-phosphatase domain is—indirectly—needed for autophagy as well. The Synj 5-phosphatase domain dephosphorylates phosphoinositides critical for endocytosis and *synj* 5-phosphatase mutants strongly disrupt endocytosis in mouse neurons (Mani *et al*, 2007). Endocytosis itself is required for the maturation of autophagic markers, suggesting that ultimately, the 5-phosphatase domain may block autophagy as well (Jäger *et al*, 2004; Hyttinen *et al*, 2013; Puri *et al*, 2013). This idea is consistent with evidence from the zebrafish study where a Synj 5-phosphatase mutant (D732A) blocks autophagy in photoreceptor neurons (George *et al*, 2016). Further experiments to determine whether this mutant, similar to data in mouse neurons, also blocks endocytosis in zebrafish or fruit flies are awaited, but the data are consistent with endocytic defects to precede autophagy. Hence, we propose a direct function of the SAC1 domain in synaptic autophagosome flux by PI(3)P and PI(3,5)P_2 dephosphorylation and a potential indirect role of the 5-phosphatase domain by mediating synaptic endocytosis.

PtdInsP phosphatase enzymes are classic drivers of organelle biogenesis and function since they alter membrane lipid

composition and thus which proteins interact with this membrane (Wenk & De Camilli, 2004; Lauwers *et al*, 2016). The biochemical basis of how Synj1 contributes to endocytosis is relatively well studied. The 5-phosphatase domain dephosphorylates PI(4,5)P_2, thereby lowering the affinity of clathrin adaptors for the membrane of newly formed vesicles and promoting synaptic vesicle uncoating (Cremona *et al*, 1999; Gad *et al*, 2000; Verstreken *et al*, 2003). Our data suggest that the Synj1 SAC1 domain that hydrolyzes PI(3)P, PI(4)P, and PI(3,5)P_2 may have a similar "uncoating" role, but acting during the early steps of autophagosome biogenesis. Indeed, it was previously established that the early-stage autophagosome membrane contains PI(3)P and PI(3,5)P_2 and that these phosphoinositides recruit PI(3)P/PI(3,5)P_2-binding proteins, like Atg18a (Simonsen & Tooze, 2009; Noda *et al*, 2010; Dall'Armi *et al*, 2013; Proikas-Cezanne *et al*, 2015). Here, we observe that synapses expressing $Synj^{RQ}$ accumulate the $Atg18a^{GFP}$ marker of early autophagosomes, but produce far fewer mature Atg8-positive structures. Furthermore, using *in vivo* CLEM for neurons expressing $Atg18a^{GFP}$, we ultrastructurally define that Atg18a is attached to cisternal-like membrane structures and these are overly abundant within $Synj^{RQ}$ synapses. Finally, live cell imaging shows that $Atg18a^{GFP}$ accumulations are immobilized within presynaptic terminals expressing $Synj^{RQ}$, suggesting that the Synj SAC1 domain normally promotes Atg18a cycling between soluble and membrane-bound pools. Note that these data are inconsistent with a direct involvement of the 5-phosphatase domain (George *et al*, 2016) as this domain is responsible for the dephosphorylation of phosphoinositide species that Atg18a does not bind to. We therefore propose a model, where Synj-mediated PI(3)P and PI(3,5)P_2 hydrolysis on nascent autophagosomes lowers the affinity for PI(3)P/PI(3,5)P_2-binding proteins, including Atg18a, to release these from the membrane. This mechanism, regulated by the synapse-enriched Synj, is similar to that thought to be mediated by myotubularin (Ymr1) during autophagy in yeast cells (Cebollero *et al*, 2012). Interestingly, WIPI2 (the Atg18a homolog) cycling is known to recruit LC3/Atg8 to autophagosomes of non-neuronal cell types (Polson *et al*, 2010; Dooley *et al*, 2014), and thus, Atg18a immobilization can explain why the Synj SAC1 activity is needed for Atg8 accumulation at synapses. Hence, we propose that cycles of Atg18a recruitment followed by Synj SAC1 domain-dependent shedding allow the recruitment and concentration of Atg8 on the synaptic autophagosomal membrane, explaining why the $Synj^{RQ}$ protein fails to support the production of mature autophagosomes.

This model of Synj1 function has parallels with the roles of the yeast myotubularin Ymr1 and INP52 and INP53 PtdInsP phosphatases in autophagosome biogenesis (Parrish *et al*, 2004; Cebollero *et al*, 2012; Cheng *et al*, 2014), which provides conceptual support to our finding that the PI(3)P phosphatase activity of Synj operates in autophagy at synapses. Given that Synj is presynaptic, we hypothesize that a different PI(3)P/PI(3,5)P_2-hydrolyzing enzyme mediates autophagosome maturation in non-neuronal animal cells and neuronal cell bodies. In addition, our data do not preclude the possibility that PtdInsP dephosphorylation mediated by the Synj1 SAC1 domain also contributes to other cell biological processes, potentially including endocytosis under certain conditions, but thus far, we have found no evidence for this. It is intriguing to consider the evolutionary consequences of combining 5-phosphatase and SAC1 domains in Synj proteins throughout the animal kingdom. This is consistent with the idea that both domains contribute to a cell biological process, perhaps acting sequentially to drive multiple stages of organelle maturation. Alternatively, it is possible that the dual roles of Synj allow this protein to couple autophagy to levels of synaptic vesicle cycling, and thus ensure sufficient protein turnover depending on the level of synaptic activity.

Our data connect impaired presynaptic autophagy to PD pathology. This is consistent with the classical concept of abnormal protein homeostasis causing proteopathic stress and driving neurodegenerative disease. However, this role of Synj highlights the concept that protein homeostasis within presynaptic terminals has a particularly important role in these diseases. We demonstrate that the pathogenic R258Q mutation in the presynaptic PD protein SYNJ1 impairs synaptic macroautophagy, and we associate this with neurodegeneration including loss of dopaminergic neurons. Another presynaptic PD protein alpha-synuclein affects membrane trafficking (Chua & Tang, 2011; Soper *et al*, 2011), although its roles remain less well defined than those of Synj. The PD proteins Parkin and Pink1 are thought to drive mitophagy, a specialized form of macroautophagy that targets mitochondria for degradation (Narendra *et al*, 2008; Kawajiri *et al*, 2010; Vincow *et al*, 2013). In addition, LRRK2, the most commonly mutated protein in PD, also affects autophagy within synaptic terminals (Soukup *et al*, 2016). In the case of LRRK2, this appears to occur via the essential presynaptic membrane factor EndophilinA (Soukup *et al*, 2016) that, interestingly, is a key regulator of Synj activity (Schuske *et al*, 2003; Verstreken *et al*, 2003). Future work should continue to examine whether the presynaptic terminal has a unique network of proteins that control macroautophagy, a membrane-mediated mechanism to clear damaged proteins or organelles. It is important to discover whether mutations in different PD genes indeed converge onto this process and, if so, to consider synaptic autophagy as an important target for development of anti-PD therapies.

Experimental Procedures

Fly stocks and genetics

Flies were grown on standard cornmeal and molasses medium supplemented with yeast paste at 25°C. The following *Drosophila* stocks were obtained from the Bloomington Stock Center: *w; P{hs-I-CreI.R}1A Sb1/TM6, y[1] w[*]; Mi{y[+mDint2]=MIC}Synj[MI11871]/SM6a* (Venken *et al*, 2011). The following fly stocks were obtained from the laboratory where the stock was first described: *w;UAS-mCherry-Atg8a* (Chang & Neufeld, 2009), *UAS GFP::Lamp1/CyO;TM6B/Sb bos1* (Pulipparacharuvil *et al*, 2005), *w;; UAS-PLCd-PH-EGFP* (Verstreken *et al*, 2009), *yw,eyFLP GMR-LacZ; FRT42D* $synj^1$*/CyO, and yw,eyFLP GMR-LacZ;FRT42D* $synj^2$*/CyO* (Verstreken *et al*, 2003), *w;;atg18a(W3)/TM6b,Hu,Tb and w;;atg18a(W4)/TM6b,Hu,Tb* (Shen & Ganetzky, 2009), genomic *w;;* $Atg9^{HA}$ (G. Juhász, unpublished).

Transgenic flies

A list of fly genotypes used in this study can be found in the Appendix Supplementary Methods section. All constructs were

generated using a seamless cloning method (Gibson Assembly, NEB). *UAS synj^{RQ}*, *UAS synj^{CS}*, and *UAS synj^{+}* were created using gBlocks (Integrated DNA Technologies, Inc.) and PCR products generated using primers listed in the Appendix Supplementary Methods section from CH322-135G1 P[acman] plasmid [BACPAC Resources Center (BPRC)] (Venken *et al*, 2006, 2009), cloned into the EcoRI site of pUAST-attB, sequence-verified, and inserted into attP site VK37 (22A3) using PhiC31-mediated integration at BestGene Inc.

synj^{RQ} knock-in flies were created as described in Vilain *et al* (2014). Targeting vector MiMIC 1322 pBS-KS-attB1-2 I-SceI Synj^{RQ} I-CreI was generated using primers listed in the Appendix Supplementary Methods section from CH322-135G21 P[acman] plasmid (BPRC) and cloned first into XhoI and PstI sites of pSV004 (containing I-SceI and I-CreI sites, see Appendix Supplementary Methods section) followed by restriction with SmaI, gel purification, and cloning into BbsI sites of MiMIC 1322 pBS-KS-attB1-2 vector with an additional linker sequence containing BbsI sites (see Appendix Supplementary Methods section) into XbaI and EcoRI sites. Next, the construct was inserted into flies with Mi{MIC}Synj^{MI11871} using PhiC31-mediated integration by in-house injection. Efficiencies were 30% for integration into the Mi{MIC}Synj^{MI11871}, 15% for desired orientation, and 37% of I-CreI double-strand break/repair. After genomic manipulation, the whole locus was sequence-verified.

UAS GFP::Atg18a, *UAS GFP::Atg18b*, *UAS GFP::CG11975, UAS mEOS3.2::Atg18a*, *UAS eGFP-mCherry::Atg8a* were created using gBlocks (Integrated DNA Technologies, Inc.) and PCR products generated using primers listed in the Appendix Supplementary Methods section, all Atg18 homologues cDNAs as template were obtained from the Proteomic ORF Collection (Yu *et al*, 2011) (respectively, LD38705, GH07816, and LD32381), mEOS3.2 was PCR from Addgene plasmid #54550 and cloned into the XhoI site of pUAST-attB, and Atg8 was cloned in between the EcoRI and XbaI sites of pUAST-attB. All constructs were sequence-verified and inserted into attP site VK20 (99F8) using PhiC31-mediated integration at BestGene Inc or by in-house injection.

Induction of autophagy by starvation, electrical stimulation, and chloroquine assay

Autophagy induction and flux assay were performed by placing early third-instar larvae on petri dishes containing 20% sucrose and 1% agarose for 3–4 h prior to experimentation (Scott *et al*, 2004). Electrical stimulation, 20 Hz for 30 min, to induce autophagy was conducted as described before (Soukup *et al*, 2016). For the chloroquine assay, we fed third-instar larvae 4 h on standard and starvation food containing 10 mg/ml chloroquine diphosphate salt (Sigma).

Correlative light and electron microscopic studies (CLEM and TEM)

Correlative light and electron microscopy studies were performed as described in Soukup *et al* (2016). Before dissection in HL3, larvae were starved for 3–4 h. The samples were directly fixed for 2 h at room temperature in the dark (0.5% glutaraldehyde, 2% paraformaldehyde in 0.1 M phosphate buffer, pH = 7.2), followed by washing steps in 0.1 M phosphate buffer, pH = 7.2. near-infrared branding (NIRB) was performed on a LSM 710 upright confocal microscope using the bleaching function as described (Urwyler *et al*, 2015). Before and after NIRB, z-stacks of the region of interest were acquired. Next, larvae were post-fixed in 1% glutaraldehyde, 2% paraformaldehyde in 0.1 M phosphate buffer, pH = 7.2 at 4°C overnight or until further processing as described in Fernandes *et al* (2014). NIRB introduced branding marks were used as a guide to identify *Drosophila* NMJ boutons previously imaged with the confocal microscope. Electron and fluorescent micrographs overlay, and identification of Atg18a^{GFP}-positive ultrastructural features and processing of micrographs using brightness and contrast were performed with NIH ImageJ and Adobe Photoshop Elements 14.

TEM studies of larval boutons were performed as described in Kasprowicz *et al* (2008). Larvae were starved for 3–4 h prior to dissection and fixation. TEM of the adult fly heads was performed as described previously in Slabbaert *et al* (2016).

Imaging and quantification

For live imaging of Atg8^{mCherry}, Atg8$^{GFP\text{-}mCherry}$, Atg18a^{GFP}, Atg18b^{GFP}, CG11975^{GFP}, or Lamp1^{GFP}, larvae expressing these markers were dissected in HL3 on sylgard plates and imaged on a Nikon A1R confocal microscope with a 60× NA 1.0 water-dipping lens. All images were collected with a pinhole of 1 airy unit and a resolution of 1,024 × 1,024. Imaging settings between experiments with the same marker were identical. Images are shown either in grayscale or using a 16-color lookup table (the LUT is shown in the figure).

Quantification of number of puncta or intensity was performed in NIH ImageJ. Atg8^{mCherry}, Atg8$^{GFP\text{-}mCherry}$, Atg18a^{GFP}, or CG11975^{GFP} dots were counted using particle analysis of a binary image combined with applying a threshold mask on the cytoplasmic signal to calculate the bouton area. Lamp1^{GFP} fluorescence intensities were measured by first applying a threshold to mark the boutonic areas followed by measuring the average pixel intensities in boutonic areas. The different conditions were blinded before imaging and quantifying the data.

Fluorescence recovery after photobleaching (FRAP) was performed on third-instar larval fillets dissected in HL3 on sylgard-coated plates using a protocol adapted from Seabrooke *et al* (2010). Experiments were conducted on a Nikon A1R confocal microscope with a 60× NA 1.0 water-dipping lens. Before bleaching, 10 images were acquired to set the pre-bleach intensity. Next, bleaching (minimum 50% of the pre-bleach intensity, by two rapidly iterated laser bursts), using a 488-nm laser, was focused on an Atg18a^{GFP} dot, directly followed by image acquisition for 120 s (60 scans with a 2,12-s interval). The fluorescence intensity of the selected Atg18a^{GFP} dot was analyzed in NIH ImageJ.

Photoconversion of mEOS3.2 was performed on third-instar larval fillets dissected in HL3 on sylgard-coated plates; next, nerves were cut in HL3 with NAS (100 μM) followed by mounting the larval prep on a glass slide in HL3 with NAS. Experiments were conducted on a Nikon A1R confocal microscope with a 60× NA1.4 oil lens; all images were collected with an open pinhole and a resolution of 1,024 × 1,024. Images of the Atg18a$^{mEOS3.2}$ dot of interest were taken before, directly after, and 5 and 10 min after photoconversion (conducted using a 405-nm laser) of the neighboring bouton. The fluorescence intensity of the selected Atg18a$^{mEOS3.2}$ dot was analyzed in NIH ImageJ.

Single-particle tracking photoactivation localization microscopy (sptPALM)

SptPALM was carried out on transgenic Atg18a$^{mEOS3.2}$ third-instar *Drosophila* larvae dissected on sylgard base as previously described (Bademosi *et al*, 2017). Briefly, Atg18a$^{mEOS3.2}$ was imaged at the larva NMJ on muscles 6 and 7 of the second abdominal segments, using total internal reflection (TIRF) microscopy under oblique illumination. Dissected larvae on the sylgard base were inverted onto glass-bottomed imaging dishes (In Vitro Scientific). Localization and tracking of single Atg18a$^{mEOS3.2}$ molecules were carried out using a 63× water-immersion objective (1.2 numerical aperture, C-Apochromat) on the ELYRA PS.1 microscope (Zeiss). NMJs were located using 488-nm laser (18.72 mW) illumination. A 405-nm laser (0.6 mW) was used for photoconversion, while imaging of photoconverted Atg18a$^{mEOS3.2}$ molecules was done using 561-nm laser (20.6 mW) to spatially visualize and temporally distinguish individual molecules (405-nm laser was used at 0.009–0.3% power, while 75% power was used for 561 nm). Single-molecule fluorescence was collected by a sensitive electron-multiplying charge-coupled device (EMCCD) camera (Evolve, Photometric). Zen Black acquisition software (2012 version, Carl Zeiss) was used for movie acquisition. Images were captured at 33 Hz and 15,000 frames were obtained per NMJ. sptPALM analysis is described in Appendix Supplementary Methods section.

Complete starvation

Complete starvation assay was performed as described in Juhász *et al* (2007), briefly 1-day-old fed flies were transferred to vials containing a gel of water (1% agarose in water) and transferred to a new vial every day. Dead flies were counted manually multiple times a day.

Light-induced degeneration

Light-induced retinal degeneration studies were performed by rearing flies for 7 days in constant illumination at 1,300 lux and 25°C (Soukup *et al*, 2013).

Visualization of TH-positive neuronal clusters after aging adult flies

Aging and visualization of dopaminergic clusters was performed by aging 1- to 3-day-old adult flies for an additional 30 days at 25°C (flies were placed on fresh medium every 3 days). At day 30, fly brains were dissected and stained (see immunohistochemistry). Images of dopaminergic clusters (labeled by the anti-TH antibody) were captured with a Nikon A1R confocal microscope using a 20× objective 0.75 NA (Nikon). The total number of TH-positive neurons throughout the brain and in both hemispheres for the PPM1, PPM2, PPM3, and PPL1 clusters was counted manually.

Neural progenitor differentiation

The iPSCs (generation and karyotyping described in Appendix Supplementary Methods and Appendix Table S1) were grown on irradiated MEFs and cultured in normal iPSC medium (DMEM/F12 Advanced (Gibco Life Technologies) supplemented with 20% KOSR, 2 mM L-glutamine, 0.1 mM MEM-NEAA, 0.1 mM 2-mercaptoethanol, 100 units/ml penicillin/streptomycin (all from Life Technologies)) and 10 ng/ml bFGF (Perprotech) at 37°C/5% CO_2. Medium was changed daily and cells were passaged every 4–6 days either mechanically or enzymatically with collagenase type IV (100 U/ml) (Life Technologies), and addition of 10 μM ROCK inhibitor (Sigma) to the medium after passaging.

Neural progenitor cells (NPCs) were created according to published protocols (de Esch *et al*, 2014; Gunhanlar *et al*, 2017) with minor modifications. Briefly, for embryoid body (EB) generation, iPSCs were dissociated and transferred to non-adherent plates in normal iPSC medium without bFGF and cultured on a shaker at 37°C/5% CO_2. After 2 days *in vitro* (DIV), medium was replaced by neural induction medium (DMEM/F12 Advanced, 1:100 N2 supplement, 100 units/ml penicillin/streptomycin (all from Life Technologies) and 2 μg/ml heparin (Sigma)). After 7 DIV, the EBs were partially dissociated and plated on laminin-coated culture dishes in neural induction medium.

Neural progenitor cells growing out of the attached EB fragments were cultured for 8 DIV at 37°C/5% CO_2, and medium was changed every other day. Subsequently, the NPCs were split between 1:2 and 1:6 with collagenase every 5–7 days and cultured on laminin (Sigma)-coated plates. The NPCs were maintained in NPC medium [DMEM/F12 Advanced, 1:100 N2 supplement, 1:50 B27-RA supplement, 100 units/ml penicillin/streptomycin (all from Life Technologies), 1 μg/ml laminin (Sigma), and 20 ng/ml bFGF (Preprotech)].

Neural differentiation

Neural progenitor cells were passaged 1:1 to poly-D-lysine (PDL) (Sigma)- and laminin (Sigma)-coated coverslips and cultured in neural differentiation medium [Neurobasal medium supplemented with 1:100 N2 supplement, 1:50 B27 supplement, 0.1 mM MEM-NEAA, 100 units/ml penicillin/streptomycin (all from Life Technologies), 20 ng/ml BDNF (ProspecBio), 20 ng/ml GDNF (ProspecBio), 1 μM db-cAMP (Sigma), 200 μM ascorbic acid (Sigma), and 2 μg/ml laminin (Sigma)]. The differentiating cells were cultured for 28 DIV at 37°C/5% CO_2, and medium was changed every other day.

Neuron starvation

At 28 DIV, neurons were either incubated for 3 h in neural differentiation medium supplemented with 100 μM leupeptin (Roche) for the control condition, or in preconditioned EBSS (Life Technologies) supplemented with 100 μM leupeptin (Roche) for the starved condition.

Statistics

GraphPad Prism 6 (San Diego, USA.) was used to determine statistical significance. Prior to this, datasets were tested for normal distribution using a D'Agostino–Pearson Omnibus test. Next, normally distributed data were tested with parametric tests: Student's *t*-test was used when two datasets were compared and we used a one-way analysis of variance test (ANOVA) followed by a

post hoc Tukey test when more than two datasets were compared. Non-normally distributed data were tested using non-parametric tests: when comparing two datasets, we used a Mann–Whitney test, and when comparing more than two datasets, we used an ANOVA Kruskal–Wallis test followed by a Dunn's *post hoc* test. Significance levels are defined as $****P < 0.0001$, $***P < 0.001$, $**P < 0.01$, $*P < 0.05$, ns (not significant) = $P > 0.05$. "n" in the legends indicates either the number of animals used or the number of NMJs analyzed.

Expanded View for this article is available online.

Acknowledgements

We thank T. Neufeld, H. Krämer, G. Juhász, and B. Ganetzky, the Bloomington *Drosophila* Stock Center the Developmental Studies Hybridoma bank for reagents and the VIB Bio-imaging core Leuven for help and BestGene Inc for *Drosophila* embryo Injections. We thank Mehrnaz Ghazvini and Joost Gribnau from the Erasmus MC iPS core facility for generation of the iPSC lines, Bruno Van Swinderen (Queensland Brain Institute, The University of Queensland) for use of his fly facility and insightful discussions. We especially thank Rose Goodchild for excellent discussions throughout the study, Willem Van den Bergh for additional in-house injections, and Liesbeth Deaulmerie and the Verstreken laboratory members for help and consultation. Research support was provided by a Flanders Innovation Agency (IWT) Fellowship to RV (121324), KU Leuven (CREA, GOA), ERC CoG (646671), the Research Foundation Flanders (FWO grants G088515N, G094915N, G0D3317N, G0D3417N), the Hercules Foundation, the Interuniversity Attraction Pole program by BELSPO (P7/16), a Methusalem grant of the Flemish government, VIB, the Vlaamse Parkinson Liga, the Stichting ParkinsonFonds (the Netherlands), the Dorpmans-Wigmans Stichting, an Erasmus MC MRace promotie grant to VB and WM, the EU Joint Programme—Neurodegenerative Disease Research (JPND) Memorabel (733051065) supported by the Nederlandse organisatie voor gezondheidsonderzoek en zorginnovatie (ZonMw) under the aegis of JPND to VB and an Hersenstichting Fellowship to FdV, the National Health and Medical Research Council (NHMRC) project grant (GNT1120381 to FAM) and Australian Research Council LIEF Grants (LE0882864 and LE130100078 to FAM). FAM is a National Health and Medical Research Council Senior Research Fellow (GNT1060075).

Author contributions

RV, SFS, and PV conceived the study. RV, SFS, and PV analyzed data and wrote the paper. RV, SK, RM, AB, JM, NS, LB, SG, JS, SV, MP, PB, STM, FMSdV, SAK, NVG, WM, VB, FAM, SFS, and PV performed experiments and/or provided reagents, and NS performed the in-house injection. All the authors approved the final version of the manuscript.

Conflict of interest

The authors declare that they have no conflict of interest.

References

Bademosi AT, Lauwers E, Padmanabhan P, Odierna L, Chai YJ, Papadopulos A, Goodhill GJ, Verstreken P, van Swinderen B, Meunier FA (2017) *In vivo* single-molecule imaging of syntaxin1A reveals polyphosphoinositide- and activity-dependent trapping in presynaptic nanoclusters. *Nat Commun* 8: 13660

Baskaran S, Ragusa MJ, Boura E, Hurley JH (2012) Two-site recognition of phosphatidylinositol 3-phosphate by PROPPINs in autophagy. *Mol Cell* 47: 339 – 348

Burke RE, O'Malley K (2013) Axon degeneration in Parkinson's disease. *Exp Neurol* 246: 72 – 83

Burman C, Ktistakis NT (2010) Regulation of autophagy by phosphatidylinositol 3-phosphate. *FEBS Lett* 584: 1302 – 1312

Cebollero E, van der Vaart A, Zhao M, Rieter E, Klionsky DJ, Helms JB, Reggiori F (2012) Phosphatidylinositol-3-phosphate clearance plays a key role in autophagosome completion. *Curr Biol* 22: 1545 – 1553

Chang Y-Y, Neufeld TP (2009) An Atg1/Atg13 complex with multiple roles in TOR-mediated autophagy regulation. *Mol Biol Cell* 20: 2004 – 2014

Cheng J, Fujita A, Yamamoto H, Tatematsu T, Kakuta S, Obara K, Ohsumi Y, Fujimoto T (2014) Yeast and mammalian autophagosomes exhibit distinct phosphatidylinositol 3-phosphate asymmetries. *Nat Commun* 5: 3207

Chi C, Zhu H, Han M, Zhuang Y, Wu X, Xu T (2010) Disruption of lysosome function promotes tumor growth and metastasis in *Drosophila*. *J Biol Chem* 285: 21817 – 21823

Chua CEL, Tang BL (2011) Rabs, SNAREs and α-synuclein–membrane trafficking defects in synucleinopathies. *Brain Res Rev* 67: 268 – 281

Cremona O, Di Paolo G, Wenk MR, Lüthi A, Kim WT, Takei K, Daniell L, Nemoto Y, Shears SB, Flavell RA, McCormick DA, De Camilli P (1999) Essential role of phosphoinositide metabolism in synaptic vesicle recycling. *Cell* 99: 179 – 188

Dall'Armi C, Devereaux KA, Di Paolo G (2013) The role of lipids in the control of autophagy. *Curr Biol* 23: R33 – R45

Devereaux K, Dall'Armi C, Alcazar-Roman A, Ogasawara Y, Zhou X, Wang F, Yamamoto A, De Camilli P, Di Paolo G (2013) Regulation of mammalian autophagy by class II and III PI 3-kinases through PI3P synthesis. *PLoS One* 8: e76405

DeVorkin L, Gorski SM (2014) Monitoring autophagy in *Drosophila* using fluorescent reporters in the UAS-GAL4 system. *Cold Spring Harb Protoc* 2014: pdb.prot080341

Di Paolo G, De Camilli P (2006) Phosphoinositides in cell regulation and membrane dynamics. *Nature* 443: 651 – 657

Dickman DK, Lu Z, Meinertzhagen IA, Schwarz TL (2006) Altered synaptic development and active zone spacing in endocytosis mutants. *Curr Biol* 16: 591 – 598

Dooley HC, Razi M, Polson HEJ, Girardin SE, Wilson MI, Tooze SA (2014) WIPI2 links LC3 conjugation with PI3P, autophagosome formation, and pathogen clearance by recruiting Atg12-5-16L1. *Mol Cell* 55: 238 – 252

de Esch CEF, Ghazvini M, Loos F, Schelling-Kazaryan N, Widagdo W, Munshi ST, van der Wal E, Douben H, Gunhanlar N, Kushner SA, Pijnappel WWMP, de Vrij FMS, Geijsen N, Gribnau J, Willemsen R (2014) Epigenetic characterization of the FMR1 promoter in induced pluripotent stem cells from human fibroblasts carrying an unmethylated full mutation. *Stem Cell Reports* 3: 548 – 555

Fernandes AC, Uytterhoeven V, Kuenen S, Wang Y-C, Slabbaert JR, Swerts J, Kasprowicz J, Aerts S, Verstreken P (2014) Reduced synaptic vesicle protein degradation at lysosomes curbs TBC1D24/sky-induced neurodegeneration. *J Cell Biol* 207: 453 – 462

Gad H, Ringstad N, Löw P, Kjaerulff O, Gustafsson J, Wenk M, Di Paolo G, Nemoto Y, Crun J, Ellisman MH, De Camilli P, Shupliakov O, Brodin L (2000) Fission and uncoating of synaptic clathrin-coated vesicles are perturbed by disruption of interactions with the SH3 domain of endophilin. *Neuron* 27: 301 – 312

George AA, Hayden S, Stanton GR, Brockerhoff SE (2016) Arf6 and the 5′ phosphatase of synaptojanin 1 regulate autophagy in cone photoreceptors. *Inside Cell* 1: 117 – 133

Gunhanlar N, Shpak G, van der Kroeg M, Gouty-Colomer LA, Munshi ST, Lendemeijer B, Ghazvini M, Dupont C, Hoogendijk WJ, Gribnau J, de Vrij

FMS, Kushner SA (2017) A simplified protocol for differentiation of electrophysiologically mature neuronal networks from human induced pluripotent stem cells. *Mol Psychiatry* in press. doi: 10.1038/mp.2017.56.

Guo S, Stolz LE, Lemrow SM, York JD (1999) SAC1-like domains of yeast SAC1, INP52, and INP53 and of human synaptojanin encode polyphosphoinositide phosphatases. *J Biol Chem* 274: 12990 – 12995

Harris TW, Hartwieg E, Horvitz HR, Jorgensen EM (2000) Mutations in synaptojanin disrupt synaptic vesicle recycling. *J Cell Biol* 150: 589 – 600

He C, Song H, Yorimitsu T, Monastyrska I, Yen W-L, Legakis JE, Klionsky DJ (2006) Recruitment of Atg9 to the preautophagosomal structure by Atg11 is essential for selective autophagy in budding yeast. *J Cell Biol* 175: 925 – 935

Heidelberger R, Thoreson WB, Witkovsky P (2005) Synaptic transmission at retinal ribbon synapses. *Prog Retin Eye Res* 24: 682 – 720

Hernandez D, Torres CA, Setlik W, Cebrián C, Mosharov EV, Tang G, Cheng HC, Kholodilov N, Yarygina O, Burke RE, Gershon M, Sulzer D (2012) Regulation of presynaptic neurotransmission by macroautophagy. *Neuron* 74: 277 – 284

Hyttinen JMT, Niittykoski M, Salminen A, Kaarniranta K (2013) Maturation of autophagosomes and endosomes: a key role for Rab7. *Biochim Biophys Acta* 1833: 503 – 510

Jäger S, Bucci C, Tanida I, Ueno T, Kominami E, Saftig P, Eskelinen E-L (2004) Role for Rab7 in maturation of late autophagic vacuoles. *J Cell Sci* 117: 4837 – 4848

Juhász G, Erdi B, Sass M, Neufeld TP (2007) Atg7-dependent autophagy promotes neuronal health, stress tolerance, and longevity but is dispensable for metamorphosis in *Drosophila*. *Genes Dev* 21: 3061 – 3066

Juhász G, Hill JH, Yan Y, Sass M, Baehrecke EH, Backer JM, Neufeld TP (2008) The class III PI(3)K Vps34 promotes autophagy and endocytosis but not TOR signaling in *Drosophila*. *J Cell Biol* 181: 655 – 666

Kabeya Y, Mizushima N, Ueno T, Yamamoto A, Kirisako T, Noda T, Kominami E, Ohsumi Y, Yoshimori T (2000) LC3, a mammalian homologue of yeast Apg8p, is localized in autophagosome membranes after processing. *EMBO J* 19: 5720 – 5728

Kasprowicz J, Kuenen S, Miskiewicz K, Habets RLP, Smitz L, Verstreken P (2008) Inactivation of clathrin heavy chain inhibits synaptic recycling but allows bulk membrane uptake. *J Cell Biol* 182: 1007 – 1016

Kawajiri S, Saiki S, Sato S, Sato F, Hatano T, Eguchi H, Hattori N (2010) PINK1 is recruited to mitochondria with parkin and associates with LC3 in mitophagy. *FEBS Lett* 584: 1073 – 1079

Kirola L, Behari M, Shishir C, Thelma BK (2016) Identification of a novel homozygous mutation Arg459Pro in SYNJ1 gene of an Indian family with autosomal recessive juvenile Parkinsonism. *Parkinsonism Relat Disord* 31: 124 – 128

Klein C, Westenberger A (2012) Genetics of Parkinson's disease. *Cold Spring Harb Perspect Med* 2: a008888

Komatsu M, Waguri S, Chiba T, Murata S, Iwata J, Tanida I, Ueno T, Koike M, Uchiyama Y, Kominami E, Tanaka K (2006) Loss of autophagy in the central nervous system causes neurodegeneration in mice. *Nature* 441: 880 – 884

Krebs CE, Karkheiran S, Powell JC, Cao M, Makarov V, Darvish H, Di Paolo G, Walker RH, Shahidi GA, Buxbaum JD, De Camilli P, Yue Z, Paisán-Ruiz C (2013) The Sac1 domain of SYNJ1 identified mutated in a family with early-onset progressive Parkinsonism with generalized seizures. *Hum Mutat* 34: 1200 – 1207

Lauwers E, Goodchild R, Verstreken P (2016) Membrane lipids in presynaptic function and disease. *Neuron* 90: 11 – 25

Lepeta K, Lourenco MV, Schweitzer BC, Martino Adami PV, Banerjee P, Catuara-Solarz S, de La Fuente Revenga M, Guillem AM, Haidar M, Ijomone OM, Nadorp B, Qi L, Perera ND, Refsgaard LK, Reid KM, Sabbar M, Sahoo A, Schaefer N, Sheean RK, Suska A *et al* (2016) Synaptopathies: synaptic dysfunction in neurological disorders—A review from students to students. *J Neurochem* 138: 785 – 805

Maday S, Holzbaur ELF (2014) Autophagosome biogenesis in primary neurons follows an ordered and spatially regulated pathway. *Dev Cell* 30: 71 – 85

Mani M, Lee SY, Lucast L, Cremona O, Di Paolo G, De Camilli P, Ryan TA (2007) The dual phosphatase activity of synaptojanin1 is required for both efficient synaptic vesicle endocytosis and reavailability at nerve terminals. *Neuron* 56: 1004 – 1018

Marat AL, Haucke V (2016) Phosphatidylinositol 3-phosphates-at the interface between cell signalling and membrane traffic. *EMBO J* 35: 561 – 579

Marzella L, Ahlberg J, Glaumann H (1982) Isolation of autophagic vacuoles from rat liver: morphological and biochemical characterization. *J Cell Biol* 93: 144 – 154

McPherson PS, Garcia EP, Slepnev VI, David C, Zhang X, Grabs D, Sossin WS, Bauerfeind R, Nemoto Y, De Camilli P (1996) A presynaptic inositol-5-phosphatase. *Nature* 379: 353 – 357

Narendra D, Tanaka A, Suen D-F, Youle RJ (2008) Parkin is recruited selectively to impaired mitochondria and promotes their autophagy. *J Cell Biol* 183: 795 – 803

Noda T, Matsunaga K, Taguchi-Atarashi N, Yoshimori T (2010) Regulation of membrane biogenesis in autophagy via PI3P dynamics. *Semin Cell Dev Biol* 21: 671 – 676

Olgiati S, De Rosa A, Quadri M, Criscuolo C, Breedveld GJ, Picillo M, Pappatà S, Quarantelli M, Barone P, De Michele G, Bonifati V (2014) PARK20 caused by SYNJ1 homozygous Arg258Gln mutation in a new Italian family. *Neurogenetics* 15: 183 – 188

Parrish WR, Stefan CJ, Emr SD (2004) Essential role for the myotubularin-related phosphatase Ymr1p and the synaptojanin-like phosphatases Sjl2p and Sjl3p in regulation of phosphatidylinositol 3-phosphate in yeast. *Mol Biol Cell* 15: 3567 – 3579

Paus T, Pesaresi M, French L (2014) White matter as a transport system. *Neuroscience* 276: 117 – 125

Polson HEJ, de Lartigue J, Rigden DJ, Reedijk M, Urbé S, Clague MJ, Tooze SA (2010) Mammalian Atg18 (WIPI2) localizes to omegasome-anchored phagophores and positively regulates LC3 lipidation. *Autophagy* 6: 506 – 522

Proikas-Cezanne T, Takacs Z, Dönnes P, Kohlbacher O (2015) WIPI proteins: essential PtdIns3P effectors at the nascent autophagosome. *J Cell Sci* 128: 207 – 217

Pulipparacharuvil S, Akbar MA, Ray S, Sevrioukov EA, Haberman AS, Rohrer J, Krämer H (2005) *Drosophila* Vps16A is required for trafficking to lysosomes and biogenesis of pigment granules. *J Cell Sci* 118: 3663 – 3673

Puri C, Renna M, Bento CF, Moreau K, Rubinsztein DC (2013) Diverse autophagosome membrane sources coalesce in recycling endosomes. *Cell* 154: 1285 – 1299

Quadri M, Fang M, Picillo M, Olgiati S, Breedveld GJ, Graafland J, Wu B, Xu F, Erro R, Amboni M, Pappatà S, Quarantelli M, Annesi G, Quattrone A, Chien HF, Barbosa ER, International Parkinsonism Genetics Network, Oostra BA, Barone P, Wang J *et al* (2013) Mutation in the SYNJ1 gene associated with autosomal recessive, early-onset Parkinsonism. *Hum Mutat* 34: 1208 – 1215

Ramaswami M, Krishnan KS, Kelly RB (1994) Intermediates in synaptic vesicle recycling revealed by optical imaging of *Drosophila* neuromuscular junctions. *Neuron* 13: 363 – 375

Schirinzi T, Madeo G, Martella G, Maltese M, Picconi B, Calabresi P, Pisani A (2016) Early synaptic dysfunction in Parkinson's disease: insights from animal models. *Mov Disord* 31: 802 – 813

Schuske KR, Richmond JE, Matthies DS, Davis WS, Runz S, Rube DA, van der Bliek AM, Jorgensen EM (2003) Endophilin is required for synaptic vesicle endocytosis by localizing synaptojanin. *Neuron* 40: 749 – 762

Scott RC, Schuldiner O, Neufeld TP (2004) Role and regulation of starvation-induced autophagy in the *Drosophila* fat body. *Dev Cell* 7: 167 – 178

Seabrooke S, Qiu X, Stewart BA (2010) Nonmuscle Myosin II helps regulate synaptic vesicle mobility at the *Drosophila* neuromuscular junction. *BMC Neurosci* 11: 37

Selkoe DJ (2002) Alzheimer's disease is a synaptic failure. *Science* 298: 789 – 791

Shen W, Ganetzky B (2009) Autophagy promotes synapse development in *Drosophila*. *J Cell Biol* 187: 71 – 79

Simonsen A, Tooze SA (2009) Coordination of membrane events during autophagy by multiple class III PI3-kinase complexes. *J Cell Biol* 186: 773 – 782

Slabbaert JR, Kuenen S, Swerts J, Maes I, Uytterhoeven V, Kasprowicz J, Fernandes AC, Blust R, Verstreken P (2016) Shawn, the *Drosophila* homolog of SLC25A39/40, is a mitochondrial carrier that promotes neuronal survival. *J Neurosci* 36: 1914 – 1929

Soper JH, Kehm V, Burd CG, Bankaitis VA, Lee VM-Y (2011) Aggregation of α-synuclein in *S. cerevisiae* is associated with defects in endosomal trafficking and phospholipid biosynthesis. *J Mol Neurosci* 43: 391 – 405

Soukup S-F, Pocha SM, Yuan M, Knust E (2013) DLin-7 is required in postsynaptic lamina neurons to prevent light-induced photoreceptor degeneration in *Drosophila*. *Curr Biol* 23: 1349 – 1354

Soukup S-F, Kuenen S, Vanhauwaert R, Manetsberger J, Hernández-Díaz S, Swerts J, Schoovaerts N, Vilain S, Gounko NV, Vints K, Geens A, De Strooper B, Verstreken P (2016) A LRRK2-dependent endophilina phosphoswitch is critical for macroautophagy at presynaptic terminals. *Neuron* 92: 829 – 844

Stauber WT, Hedge AM, Trout JJ, Schottelius BA (1981) Inhibition of lysosomal function in red and white skeletal muscles by chloroquine. *Exp Neurol* 71: 295 – 306

Stavoe AKH, Hill SE, Hall DH, Colón-Ramos DA (2016) KIF1A/UNC-104 transports ATG-9 to regulate neurodevelopment and autophagy at synapses. *Dev Cell* 38: 171 – 185

Tamura H, Shibata M, Koike M, Sasaki M, Uchiyama Y (2010) Atg9A protein, an autophagy-related membrane protein, is localized in the neurons of mouse brains. *J Histochem Cytochem* 58: 443 – 453

Thomas B, Beal MF (2007) Parkinson's disease. *Hum Mol Genet* 16 Spec No: R183 – R194

Tsujishita Y, Guo S, Stolz LE, York JD, Hurley JH (2001) Specificity determinants in phosphoinositide dephosphorylation: crystal structure of an archetypal inositol polyphosphate 5-phosphatase. *Cell* 105: 379 – 389

Ueda Y (2014) The role of phosphoinositides in synapse function. *Mol Neurobiol* 50: 821 – 838

Urwyler O, Izadifar A, Dascenco D, Petrovic M, He H, Ayaz D, Kremer A, Lippens S, Baatsen P, Guérin CJ, Schmucker D (2015) Investigating CNS synaptogenesis at single-synapse resolution by combining reverse genetics with correlative light and electron microscopy. *Development* 142: 394 – 405

Van Epps HA, Yim CM, Hurley JB, Brockerhoff SE (2001) Investigations of photoreceptor synaptic transmission and light adaptation in the zebrafish visual mutant nrc. *Invest Ophthalmol Vis Sci* 42: 868 – 874

Van Epps HA, Hayashi M, Lucast L, Stearns GW, Hurley JB, De Camilli P, Brockerhoff SE (2004) The zebrafish nrc mutant reveals a role for the polyphosphoinositide phosphatase synaptojanin 1 in cone photoreceptor ribbon anchoring. *J Neurosci* 24: 8641 – 8650

Vanhauwaert R, Verstreken P (2015) Flies with Parkinson's disease. *Exp Neurol* 274: 42 – 51

Verstreken P, Kjaerulff O, Lloyd TE, Atkinson R, Zhou Y, Meinertzhagen IA, Bellen HJ (2002) Endophilin mutations block clathrin-mediated endocytosis but not neurotransmitter release. *Cell* 109: 101 – 112

Verstreken P, Koh T-W, Schulze KL, Zhai RG, Hiesinger PR, Zhou Y, Mehta SQ, Cao Y, Roos J, Bellen HJ (2003) Synaptojanin is recruited by endophilin to promote synaptic vesicle uncoating. *Neuron* 40: 733 – 748

Venken KJT, He Y, Hoskins RA, Bellen HJ (2006) P[acman]: a BAC transgenic platform for targeted insertion of large DNA fragments in *D. melanogaster*. *Science* 314: 1747 – 1751

Venken KJT, Carlson JW, Schulze KL, Pan H, He Y, Spokony R, Wan KH, Koriabine M, de Jong PJ, White KP, Bellen HJ, Hoskins RA (2009) Versatile P [acman] BAC libraries for transgenesis studies in *Drosophila melanogaster*. *Nat Methods* 6: 431 – 434

Verstreken P, Ohyama T, Haueter C, Habets RLP, Lin YQ, Swan LE, Ly CV, Venken KJT, De Camilli P, Bellen HJ (2009) Tweek, an evolutionarily conserved protein, is required for synaptic vesicle recycling. *Neuron* 63: 203 – 215

Venken KJT, Schulze KL, Haelterman NA, Pan H, He Y, Evans-Holm M, Carlson JW, Levis RW, Spradling AC, Hoskins RA, Bellen HJ (2011) MiMIC: a highly versatile transposon insertion resource for engineering *Drosophila melanogaster* genes. *Nat Methods* 8: 737 – 743

Vilain S, Vanhauwaert R, Maes I, Schoovaerts N, Zhou L, Soukup S, da Cunha R, Lauwers E, Fiers M, Verstreken P (2014) Fast and efficient *Drosophila melanogaster* gene knock-ins using MiMIC transposons. *G3 (Bethesda)* 4: 2381 – 2387

Vincow ES, Merrihew G, Thomas RE, Shulman NJ, Beyer RP, MacCoss MJ, Pallanck LJ (2013) The PINK1-Parkin pathway promotes both mitophagy and selective respiratory chain turnover *in vivo*. *Proc Natl Acad Sci USA* 110: 6400 – 6405

Wang T, Martin S, Papadopulos A, Harper CB, Mavlyutov TA, Niranjan D, Glass NR, Cooper-White JJ, Sibarita J-B, Choquet D, Davletov B, Meunier FA (2015) Control of autophagosome axonal retrograde flux by presynaptic activity unveiled using botulinum neurotoxin type a. *J Neurosci* 35: 6179 – 6194

Wang T, Martin S, Nguyen TH, Harper CB, Gormal RS, Martínez-Mármol R, Karunanithi S, Coulson EJ, Glass NR, Cooper-White JJ, van Swinderen B, Meunier FA (2016) Flux of signalling endosomes undergoing axonal retrograde transport is encoded by presynaptic activity and TrkB. *Nat Commun* 7: 12976

Wenk MR, De Camilli P (2004) Protein-lipid interactions and phosphoinositide metabolism in membrane traffic: insights from vesicle recycling in nerve terminals. *Proc Natl Acad Sci USA* 101: 8262 – 8269

Whisstock JC, Romero S, Gurung R, Nandurkar H, Ooms LM, Bottomley SP, Mitchell CA (2000) The inositol polyphosphate 5-phosphatases and the apurinic/apyrimidinic base excision repair endonucleases share a common mechanism for catalysis. *J Biol Chem* 275: 37055 – 37061

Williamson WR, Wang D, Haberman AS, Hiesinger PR (2010) A dual function of V0-ATPase a1 provides an endolysosomal degradation mechanism in *Drosophila melanogaster* photoreceptors. *J Cell Biol* 189: 885 – 899

Yamamoto H, Kakuta S, Watanabe TM, Kitamura A, Sekito T, Kondo-Kakuta C, Ichikawa R, Kinjo M, Ohsumi Y (2012) Atg9 vesicles are an important membrane source during early steps of autophagosome formation. *J Cell Biol* 198: 219 – 233

Yu C, Wan KH, Hammonds AS, Stapleton M, Carlson JW, Celniker SE (2011) Development of expression-ready constructs for generation of proteomic libraries. *Methods Mol Biol* 723: 257 – 272

Zhang M, Chang H, Zhang Y, Yu J, Wu L, Ji W, Chen J, Liu B, Lu J, Liu Y, Zhang J, Xu P, Xu T (2012) Rational design of true monomeric and bright photoactivatable fluorescent proteins. *Nat Methods* 9: 727 – 729

Zhong S, Hsu F, Stefan CJ, Wu X, Patel A, Cosgrove MS, Mao Y (2012) Allosteric activation of the phosphoinositide phosphatase Sac1 by anionic phospholipids. *Biochemistry* 51: 3170 – 3177

Zhu JY, Vereshchagina N, Sreekumar V, Burbulla LF, Costa AC, Daub KJ, Woitalla D, Martins LM, Krüger R, Rasse TM (2013) Knockdown of Hsc70-5/mortalin induces loss of synaptic mitochondria in a *Drosophila* Parkinson's disease model. *PLoS One* 8: e83714